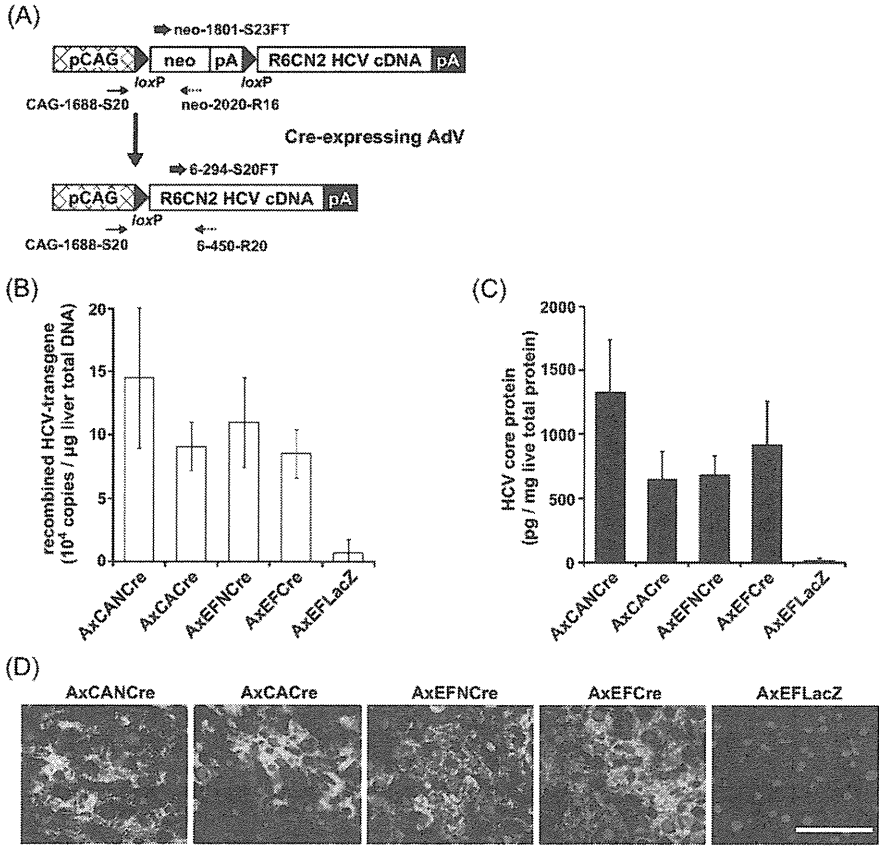

Fig. 2. Cre-mediated genomic DNA recombination and HCV core protein expression in transgenic mouse livers. (A) Structure of the Cre-mediated activation transgene unit CALNCN2 (Wakita et al., 1998). pCAG, CAG promoter; neo, neomycin-resistance gene; pA, poly(A) signal. The R6CN2 HCV cDNA (nucleotides 294–3435) contains the core, E1, E2, and NS2 regions. This construct does not allow HCV mRNA transcription prior to Cre-mediated DNA recombination, detected with the primer pair CAG-1688-S20 and neo-2020-R16. When Cre-expressing AdV is injected, the *neo* gene and poly(A) signal are removed by recombination between two *loxP* sequences. The recombined HCV transgene is detected with the primer pair CAG-1688-S20 and 6-450-R20. (B) Determination of Cre-mediated DNA recombination. CN2-29 transgenic mice were injected with 1.0×10^9 PFU for each AdV, and liver samples were harvested 7 days post-injection. Genomic DNA was extracted from the livers, and the numbers of copies of the recombined HCV-transgenes were determined using quantitative RTD-PCR with specific probes (6-294-S20FT) and a primer pair (CAG-1688-S20 and 6-450-R20). The values shown are means ± S.D. of more than three individual specimens. (C) Measurements of HCV core protein concentration in liver samples obtained from CN2-29 transgenic mice 7 days after injection of 1.0×10^9 PFU for each AdV. The samples were homogenized and the concentrations of HCV core protein were determined by EIA. The values shown are means ± S.D. of three individual specimens. (D) Immunofluorescence analysis of HCV core proteins. Liver sections of CN2-29 transgenic mice 7 days after injection of 1.0×10^9 PFU for each AdV were fixed and co-stained with rabbit anti-core polyclonal antibody (green) and DAPI (blue). Scale bar, 50 μm.

2.7. Determination of Cre-mediated HCV transgene recombination in mouse livers

The transgenic mouse livers were digested at 37 °C overnight in lysis buffer [50 mM Tris–HCl (pH 8.0), 0.1 M NaCl, 20 mM EDTA, 1% SDS] containing 1 mg/mL proteinase K. Total genomic DNA was then extracted using the phenol–chloroform extraction method. The copy numbers of the recombined HCV transgene in the livers were assessed via quantitative RTD-PCR (Takeuchi et al., 1999) with the specific probe 6-294-S20FT (5′-[FAM]-TGATAGGGTGCTTGCGAGTG-[TAMRA]-3′) and the primer pair CAG-1688-S20 (5′-GGTTGTTGTGCTGTCTCATC-3′) and 6-450-R20 (5′-ACAGGTAAACTCCACCAACG-3′) (Fig. 2A). The standard curve was generated using pCALNCN2/59-2 (Wakita et al., 1998) and quantitative RTD-PCR with the specific probe neo-1801-S23FT (5′-[FAM]-TCAAGAGACAGGATGAGGATCGT-[TAMRA]-3′) and the primer pair CAG-1688-S20 (5′-GGTTGTTGTGCTGTCTCATC-3′) and neo-2020-R16 (5′-TGCCTCGTCCTGCAGT-3′) (Fig. 2A). The *GAPDH* gene was used as an internal control for all samples. Analyses were carried out on an ABI PRISM 7700 Sequence Detection System with TaqMan Universal PCR Master Mix (Applied Biosystems).

2.8. Quantitation of HCV core proteins in mouse liver lysates

The transgenic mouse livers were homogenized in 0.5 mL RIPA buffer, and centrifuged at 15,000 rpm for 10 min at 4 °C. The protein concentrations of the supernatants were measured using the Bradford method (DC protein assay; Bio-Rad). The concentrations of HCV core proteins in the liver samples were determined using the Ortho HCV core protein ELISA kit (Eiken Chemical).

2.9. Biochemical analyses of mouse sera

Sequential blood samples were obtained by orbital bleeding after each AdV administration, and the sera were isolated by centrifugation at 10,000 rpm for 3 min at 4 °C. Serum ALT levels were determined using the Transaminase-CII Test A (Wako Pure Chemicals).

2.10. Histology and immunohistochemical staining

The liver samples were fixed with 4% paraformaldehyde in PBS, paraffin-embedded, sectioned at 4-μm thickness, and stained

with hematoxylin and eosin (H&E). Liver histology was evaluated according to modified Histology Activity Index (HAI) scores in three categories: piecemeal necrosis, spotty necrosis, and portal inflammation (Knodell et al., 1981; Yang et al., 1994).

The liver tissues were frozen in OCT compound (Tissue Tech) for immunohistochemical staining of HCV core proteins. The sections were fixed with a 1:1 solution of acetone:methanol at −20 °C for 10 min and then washed with PBS. Subsequently, the sections were incubated with the IgG fraction of an anti-HCV core rabbit polyclonal antibody (RR8) (Wakita et al., 1998) labeled with biotin in blocking buffer for 1 h at 4 °C. The sections were incubated with strept-avidin-conjugated horseradish peroxidase for 30 min at room temperature. Immunohistochemical staining was conducted using the Tyramide Signal Amplification Kit (Molecular Probes). Fluorescently labeled sections were stained with 4′,6-diamidino-2-phenylindole (DAPI; Molecular Probes) to stain the cell nuclei at room temperature before cover slipping. Fluorescence was observed under a fluorescence microscope (Carl Zeiss).

2.11. Statistical analysis

Data are shown as the mean ± S.D. Statistical analyses were performed using analysis of variance (ANOVA) followed by the Student–Newman–Keuls (SNK) test or analyzed using the unpaired Student's *t*-test. Statistical significance was established at $p < 0.05$.

3. Results

3.1. Generation of Cre-expressing AdVs

To enable HCV transgenic mice using the Cre/*lox*P system to express HCV protein persistently without severe inflammatory responses to AdV, we first constructed AdVs that expressed Cre with or without a nuclear localization signal (NLS) tag (AxEFNCre or AxEFCre, respectively) together with *LacZ* under the control of the EF1α promoter (AxEFLacZ) (Fig. 1A). AxCANCre and AxCACre were also generated to compare the impacts of using the CAG promoter and the EF1α promoter (Fig. 1A). Expression of Cre proteins from various AdVs was confirmed in human liver-derived HepG2 cells by Western blot analysis (Fig. 1B). Cre protein expression levels were not significantly different whether the gene was expressed under the control of the CAG or the EF1α promoter in the HepG2 cells (Fig. 1B). Next, we examined the recombination activities of Cre expressed via the AdVs using the Hep-CALNLZ cell line, HepG2 cells that express CALNLZ (Fig. 1C). When the Cre-expressing AdVs bearing the CAG or EF1α promoters infected these cells, the blue color produced by *LacZ* activation was observed for MOIs of 0.15–160. The cells infected with AxEFLacZ showed the blue staining in an MOI-dependent manner (Fig. 1D, lane AxEFLacZ). In contrast, the color faded for MOIs >40 when the Cre-expressing AdVs were used (Fig. 1D, lanes AxCANCre, AxCACre, AxEFNCre, and AxEFCre). At an MOI of 160, all of the Cre-expressing AdVs resulted in cytotoxicity, while the LacZ-expressing AdV did not affect cell viability (Fig. 1E).

AdV-induced immune responses are partly caused by co-expression of Ad-pIX (Nakai et al., 2007). To confirm the protein expression levels of Ad-pIX due to the AdVs, we performed Western blotting with anti-Ad-pIX sera (Fig. 1F). When HepG2 cells were infected with AdVs bearing the CAG promoter, significant amounts of Ad-pIX were detected as 14-kDa bands (Fig. 1F, lanes AxCANCre and AxCACre). In contrast, when using AdVs bearing the EF1α promoter, the 14-kDa band representing Ad-pIX was undetectable, as was the case for mock-infected HepG2 cells (Fig. 1F, lanes AxEFNCre, AxEFCre, AxEFLacZ, and mock). We also examined the mRNA expression levels of Ad-pIX and obtained similar results that correlated with the protein expression levels (Fig. 1G).

3.2. HCV gene expression and core protein production mediated by various Cre-expressing AdVs in transgenic mouse livers

The HCV transgenic mouse CN2-29 contains a reporter unit (CALNCN2) that is activated by Cre and conditionally expresses the HCV gene (Fig. 2A; Wakita et al., 1998). To assess the efficiency of Cre-expressing AdVs in promoting HCV gene expression, we intravenously injected the CN2-29 transgenic mice with various AdVs. At 7 days post-injection, Cre protein expression was confirmed by Western blot analysis of liver lysates (data not shown). The recombined HCV transgene levels in the livers were determined by quantitative RTD-PCR using specific probes and primer pairs, as described in Section 2 (Fig. 2A and B). When each Cre-expressing AdV was injected, the respective recombined HCV transgene was detectable; AxCANCre-injected CN2-29 transgenic mice expressed the highest levels of the recombined HCV transgene in their livers (Fig. 2B). CN2-29 transgenic mice injected with AdVs expressing NLS-tagged Cre had higher levels of the recombined HCV transgene in their livers (Fig. 2B, AxCANCre and AxEFNCre). This result suggests that NLS-tagged Cre efficiently translocated to the cell nucleus, which is consistent with our previous data (Baba et al., 2005). However, the levels of the recombined HCV transgene were not correlated with the expression level of HCV core protein (Fig. 2C).

The core protein levels in the livers were measured by enzyme immunoassay (EIA) as described in Section 2. The expression of the E1 and E2 proteins in the CN2-29 transgenic mouse livers has been shown previously (Wakita et al., 1998). The mean core protein level was 1.3 ng/mg total protein in the CN2-29 transgenic mouse livers 7 days after administration of AxCANCre (Fig. 2C). AxCACre- and AxEFNCre-injected mice expressed approximately one-half of the core protein levels resulting from AxCANCre injection (Fig. 2C).

Expression of core proteins in AdV-injected CN2-29 transgenic mouse livers was confirmed through immunofluorescence staining. Core proteins were expressed in the hepatocytes in the lobules of liver sections from Cre-expressing AdV-injected mice (Fig. 2D). In contrast, AxEFLacZ-injected transgenic mice did not express core proteins (Fig. 2C and D).

3.3. Liver injury and Ad-pIX expression in HCV transgenic mice injected with AdVs

To evaluate hepatocellular injury caused by expression of HCV proteins in CN2-29 transgenic mice injected with Cre-expressing AdVs, we serially estimated the serum ALT levels (Fig. 3A). For AxCANCre, the serum ALT level was elevated on day 5 and peaked 1–2 weeks post-injection (Fig. 3A, open triangle). ALT levels in AxCACre-injected transgenic mice were also elevated, although these levels declined over time (Fig. 3A, open circle). When AxEFNCre or AxEFCre was injected, ALT levels did not immediately increase, although they gradually increased after day 5 (Fig. 3A, closed triangle and closed circle, respectively). Injection of AxEFLacZ did not increase serum ALT levels in the CN2-29 transgenic mice (Fig. 3A, closed rectangle).

We also performed histological analyses of liver sections from CN2-29 transgenic mice 7 days after AdV injection (Fig. 3B). We found that severe inflammation with lymphocyte infiltration and spotty necrosis were diffusely observed in the livers of mice injected with the AdVs bearing the CAG promoter (AxCACre and AxCANCre) (Fig. 3B, a,b). In contrast, AxEFNCre-injected and AxEFCre-injected transgenic mouse livers exhibited mild inflammation without massive piecemeal necrosis on day 7 (Fig. 3B, c,d). No inflammation was observed in the AxEFLacZ-injected mice (Fig. 3B, e).

To confirm the expression levels of Ad-pIX in AdV-injected transgenic mice, we determined Ad-pIX mRNA in the liver using

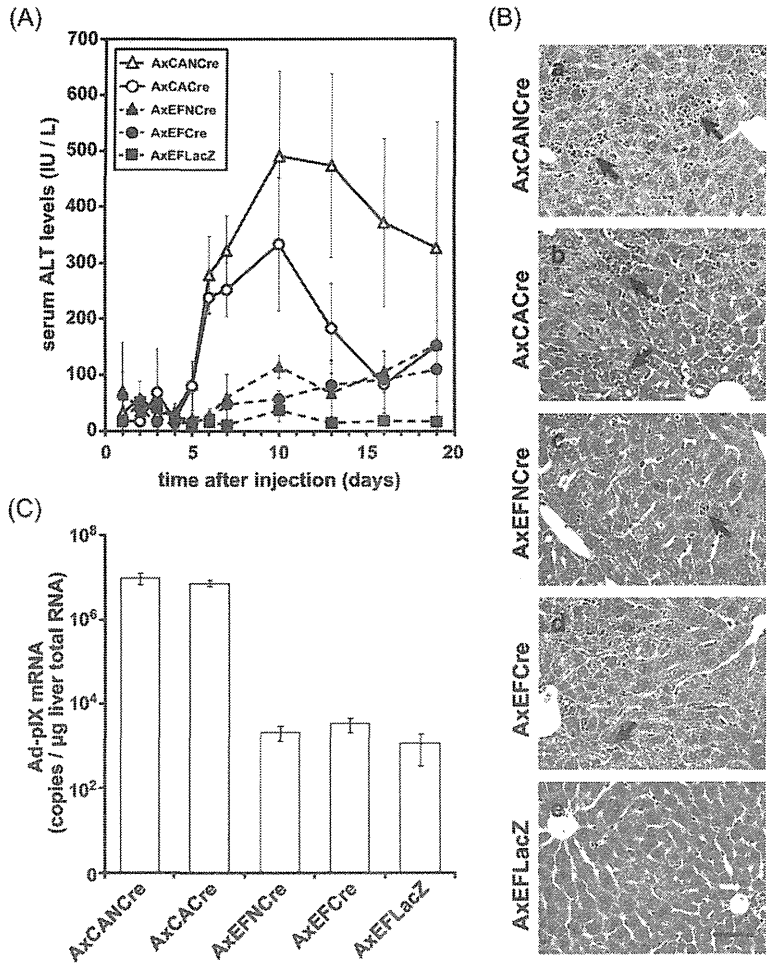

Fig. 3. Effects of AdVs on liver injuries in HCV transgenic mice. (A) Serum ALT levels were measured at the indicated time-points in CN2-29 transgenic mice injected with 1.0×10^9 PFU AxCANCre (open triangle), AxCACre (open circle), AxEFNCre (closed triangle), AxEFCre (closed circle), and AxEFLacZ (closed rectangle). The ALT levels are shown as means ± S.D. of three individual specimens. (B) Histopathologic changes in the livers of transgenic mice 7 days after injection of each AdV. The liver sections were stained with H&E. The arrows represent lymphocyte infiltrations. Scale bar, 50 μm. (C) mRNA expression of Ad-pIX in the livers. CN2-29 transgenic mice were injected with 1.0×10^9 PFU of the AdVs. After 12 h, the livers were harvested. The total RNA extracts from the livers were subjected to reverse transcription and RTD-PCR with an Ad-pIX-specific probe and a primer pair, as described in Section 2. The numbers of copies of Ad-pIX mRNA are shown as means ± S.D. of three individual specimens.

reverse transcription and quantitative RTD-PCR, as described under Section 2. The copy numbers of Ad-pIX mRNA were quite high in transgenic mice that were injected with AdV bearing the CAG promoter (Fig. 3C). The observed inflammation levels were consistent with the expression levels of Ad-pIX.

3.4. Liver inflammatory responses to the HCV protein inducibly expressed by AdVs in transgenic mice

Because our results indicated that severe liver injuries were caused by AdVs bearing the CAG promoter, we evaluated liver inflammatory responses to the HCV protein inducibly expressed by AdVs in transgenic mice 7 days post-injection according to the modified HAI scoring system (Fig. 4A) (Knodell et al., 1981; Yang et al., 1994). Among the transgenic mice, more severe liver damage was observed in those that were injected with Cre-expressing AdVs bearing the CAG promoter (Fig. 4A, AxCANCre and AxCACre) compared to those injected with Cre-expressing AdVs bearing the EF1α promoter (Fig. 4A, AxEFNCre and AxEFCre).

Because AxEFCre more efficiently expressed HCV proteins than AxEFNCre (Fig. 2C and D), we injected AxEFCre into transgenic mice and wild-type mice to examine the effects of HCV protein expression. The severity of liver inflammation in the AxEFCre-injected transgenic mice was significantly greater than in the AxEFCre-injected wild-type mice or the AxEFLacZ-injected transgenic mice (Fig. 4A and B).

Seven days after AdV administration, serum ALT levels of AxCANCre-injected wild-type mice were significantly higher than those of AxEFCre-injected wild-type mice (Fig. 4C). This ALT elevation was observed in both transgenic and wild-type mice injected with AxCANCre (Fig. 4C). In contrast, AxEFCre was injected into the two groups, transgenic mice expressing HCV proteins exhibited more severe liver injury than wild-type mice (Fig. 4C and D).

3.5. Effects of Cre-expressing AdV bearing the EF1α promoter on HCV protein expression in transgenic mouse livers

To investigate whether CN2-29 transgenic mice injected with AdVs bearing the EF1α promoter showed liver inflammation caused

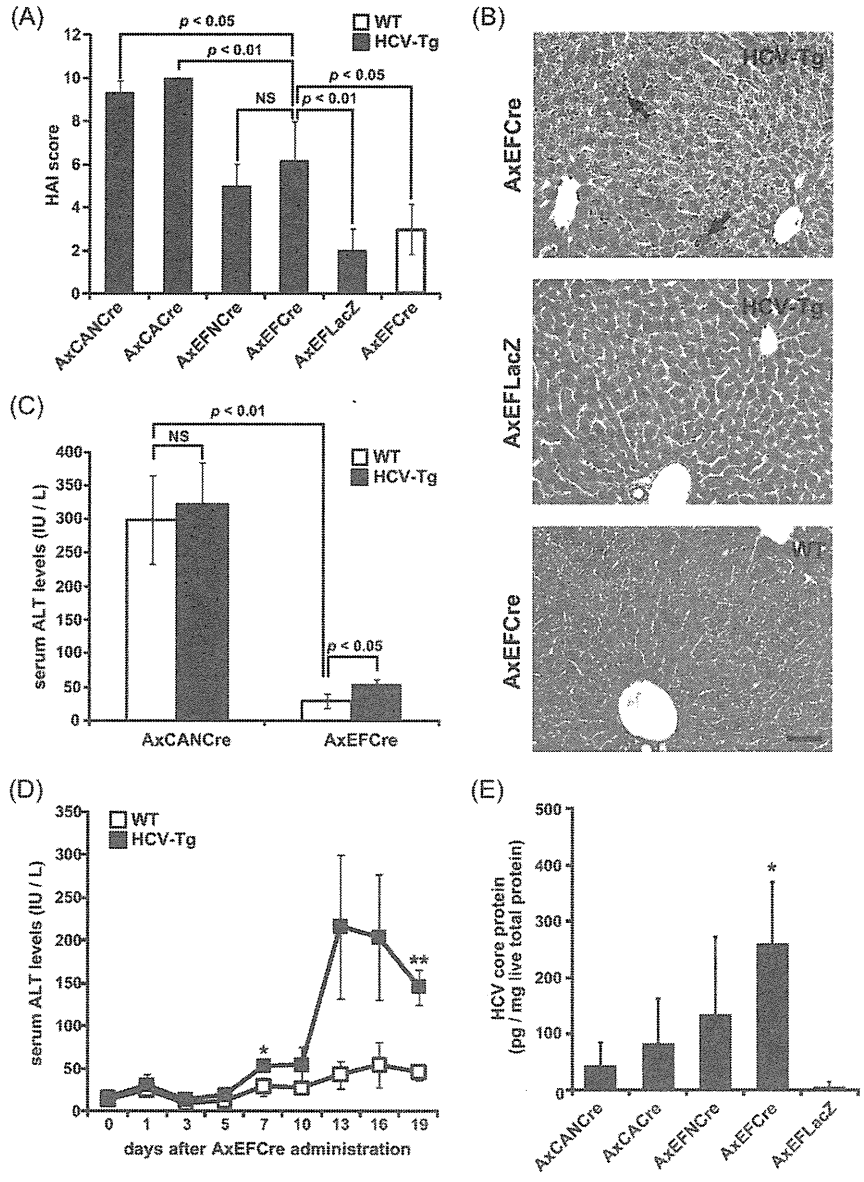

Fig. 4. Liver inflammatory responses due to HCV protein expression induced by AxEFCre. (A) Histopathology of mouse livers after injection of AdVs. Histopathologic features of the livers of CN2-29 transgenic mice (HCV-Tg, closed bars) injected with 1.0×10^9 PFU of AxCANCre, AxCACre, AxEFNCre, AxEFCre, or AxEFLacZ, and wild-type mice that were injected with 1.0×10^9 PFU of AxEFCre at day 7 post-injection (WT, opened bar). Pathologic changes were evaluated by light microscopy of H&E-stained sections of the mouse livers using the modified HAI scoring system. The extent of pathology was scored on a scale from 0 (none) to 12 (severe). All of the scores are means ± S.D. of more than three individual specimens. Statistical analysis was performed using an unpaired Student's *t*-test. NS, not significant. (B) Histopathologic changes resulting from HCV protein expression in mouse livers. CN2-29 transgenic mice (HCV-Tg) were injected with AxEFCre or AxEFLacZ and wild-type mice (WT) were injected with AxEFCre 7 days post-injection. The liver sections were stained with H&E. The arrows represent piecemeal necrosis. Scale bars, 50 μm. (C) Serum ALT levels with or without HCV protein expression 7 days after administration of the AdVs. Statistical analysis was performed using an unpaired Student's *t*-test between CN2-29 transgenic mice (HCV-Tg) and wild-type mice (WT). NS, not significant. (D) Sequential changes in serum ALT levels after AxEFCre administration. Serum ALT levels were measured at the indicated time-points in CN2-29 transgenic mice (HCV-Tg, closed square) or wild-type mice (WT, opened square) that were injected with 1.0×10^9 PFU AxEFCre. ALT levels are shown as means ± S.D. of more than three individual specimens. Statistical analysis was performed using an unpaired Student's *t*-test between CN2-29 transgenic mice (HCV-Tg) and wild-type mice (WT). $^*p < 0.05$; $^{**}p < 0.01$. (E) HCV core protein expression 21 days after AdV administration in transgenic mouse livers. CN2-29 transgenic mice were injected with 1.0×10^9 PFU for each AdV. After 21 days, the livers were harvested and homogenized. The concentrations of HCV core proteins in liver lysates were determined by EIA. The values shown are means ± S.D. of three individual experiments. Statistical analysis was performed using an ANOVA, followed by the SNK test. $^*p < 0.05$.

by persistently expressed HCV proteins, we evaluated core proteins by EIA in transgenic mouse livers 21 days post-injection of the AdVs (Fig. 4E). HCV core protein expression was scarcely detectable in the transgenic mice injected with AxCANCre, while the AxEFCre-injected transgenic mice showed significantly higher levels of core protein expression (Fig. 4E). Although, the AxCANCre injection was scarcely observed at day 21 in the transgenic mice (Fig. 4E), HCV core protein expression induced by AxEFCre injection was observed until at least day 56.

4. Discussion

In the present study, we demonstrated that Cre-expressing AdVs bearing the EF1α promoter induce HCV gene expression and

HCV protein production without induction of severe liver injury in inducible-HCV transgenic mice. We further observed that increases in serum ALT levels and liver inflammation were related to HCV protein expression mediated by AxEFCre injection. Moreover, AxEFCre injection enabled the transgenic mice to persistently express HCV proteins.

In previous studies, HCV transgenic mice constitutively expressing HCV proteins exhibited symptoms of steatosis and/or hepatocellular carcinoma, but did not show inflammatory or immunopathologic changes (Lerat et al., 2002; Moriya et al., 1997, 1998; Sun et al., 2001). Inducible-HCV transgenic mouse lineages, in which HCV protein expression is regulated, have enabled investigation of the immunopathogenesis of HCV protein expression. HCV transgenic mice regulated by the Cre/*lox*P system (Sun et al., 2005; Tumurbaatar et al., 2007; Wakita et al., 1998) or the tetracycline regulatory system (Ernst et al., 2007) exhibit inducible and liver-specific expression of HCV proteins. Inducible-HCV transgenic mice using the Cre/*lox*P system with an AdV that expresses Cre under the control of the CAG promoter (AxCANCre) exhibit HCV-specific immune responses (Wakita et al., 1998, 2000). The inducible-HCV CN2-29 transgenic mice, which express the core, E1, E2, and NS2 proteins, have HCV-specific cytotoxic T lymphocytes (Takaku et al., 2003; Wakita et al., 1998, 2000).

However, they show severe inflammatory responses to AxCANCre itself and thus, HCV protein expression is only transient (Wakita et al., 2000). These significant obstacles have limited the utility of inducible-HCV transgenic mice. Therefore, to deliver the *Cre* gene into the liver, non-adenoviral induction methods have been developed (Ho et al., 2008; Sun et al., 2005; Zhu et al., 2006). Meanwhile, adenoviral genes that cause cellular immune responses have been identified and modified AdVs that do not trigger host immune responses have been developed (Palmer and Ng, 2005). A recent study demonstrated that immune responses to AdVs bearing the CAG promoter were associated with co-expression of Ad-pIX, whereas immune responses were minimal when transgene expression was controlled by the EF1α promoter (Nakai et al., 2007). Therefore, we postulated that severe inflammation of mouse livers after administration of Cre-expressing AdVs bearing the CAG promoter (AxCANCre) might be caused by expression of Ad-pIX. In the present study, we generated Cre-expressing AdVs bearing the EF1α promoter (AxEFCre) and infected HCV transgenic mice. AxEFCre-injected mice expressed much less Ad-pIX mRNA and did not show the increased levels of ALT or severe liver inflammation as did Cre-expressing AdVs under the control of the CAG promoter (Fig. 3). In contrast, AxCANCre administration caused severe liver injury in both HCV transgenic mice and wild-type mice (Fig. 4D; Wakita et al., 2000). AxEFCre administration caused liver injury in the HCV transgenic mice, but not in the wild-type mice (Fig. 4A–D). These results suggest that AxEFCre alone induces only minimal host immune responses compared to AxCANCre; therefore, the liver inflammatory responses exhibited by AxEFCre-injected transgenic mice were clearly due to expression of HCV proteins. Because AxCANCre injection alone causes severe liver injuries, most of the hepatocytes infected with AxCANCre are eliminated and HCV protein expression in the livers of transgenic mice is only transient (Wakita et al., 2000). On the other hand, AxEFCre injection did not induce such severe liver injuries. The AxEFCre-injected HCV transgenic mice showed milder liver inflammation in response to expression of HCV proteins and persistently expressed HCV proteins without elimination of hepatocytes infected with AxEFCre.

In conclusion, HCV gene expression mediated by the Cre/*lox*P system and a Cre-expressing AdV that bears the EF1α promoter, AxEFCre, enables Cre-mediated recombination of transgenes in mice without inducing severe liver injury due to the AdV itself. Moreover, this inducible-HCV transgenic mouse model should be useful for investigation of liver injury due to HCV and the pathogenesis of HCV.

Acknowledgments

The authors wish to thank Mitsugu Takahashi for breeding the transgenic mice. This study was supported by grants from the Ministry of Education, Culture, Sports, Science and Technology of Japan; the Program for Promotion of Fundamental Studies in Health Sciences of the Pharmaceuticals and Medical Devices Agency of Japan; and the Ministry of Health, Labor and Welfare of Japan.

References

Akagi, K., Sandig, V., Vooijs, M., Van der Valk, M., Giovannini, M., Strauss, M., Berns, A., 1997. Cre-mediated somatic site-specific recombination in mice. Nucleic Acids Res. 25 (9), 1766–1773.

Baba, Y., Nakano, M., Yamada, Y., Saito, I., Kanegae, Y., 2005. Practical range of effective dose for Cre recombinase-expressing recombinant adenovirus without cell toxicity in mammalian cells. Microbiol. Immunol. 49 (6), 559–570.

Bangari, D.S., Mittal, S.K., 2006. Current strategies and future directions for eluding adenoviral vector immunity. Curr. Gene Ther. 6 (2), 215–226.

Ernst, E., Schonig, K., Bugert, J.J., Blaker, H., Pfaff, E., Stremmel, W., Encke, J., 2007. Generation of inducible hepatitis C virus transgenic mouse lines. J. Med. Virol. 79 (8), 1103–1112.

Goodman, Z.D., Ishak, K.G., 1995. Histopathology of hepatitis C virus infection. Semin. Liver Dis. 15 (1), 70–81.

Ho, K.J., Bass, C.E., Kroemer, A.H., Ma, C., Terwilliger, E., Karp, S.J., 2008. Optimized adeno-associated virus 8 produces hepatocyte-specific Cre-mediated recombination without toxicity or affecting liver regeneration. Am. J. Physiol. Gastrointest. Liver Physiol. 295 (2), G412–G419.

Kafri, T., Morgan, D., Krahl, T., Sarvetnick, N., Sherman, L., Verma, I., 1998. Cellular immune response to adenoviral vector infected cells does not require de novo viral gene expression: implications for gene therapy. Proc. Natl. Acad. Sci. U S A 95 (19), 11377–11382.

Kanegae, Y., Lee, G., Sato, Y., Tanaka, M., Nakai, M., Sakaki, T., Sugano, S., Saito, I., 1995. Efficient gene activation in mammalian cells by using recombinant adenovirus expressing site-specific Cre recombinase. Nucleic Acids Res. 23 (19), 3816–3821.

Kanegae, Y., Makimura, M., Saito, I., 1994. A simple and efficient method for purification of infectious recombinant adenovirus. Jpn. J. Med. Sci. Biol. 47 (3), 157–166.

Knodell, R.G., Ishak, K.G., Black, W.C., Chen, T.S., Craig, R., Kaplowitz, N., Kiernan, T.W., Wollman, J., 1981. Formulation and application of a numerical scoring system for assessing histological activity in asymptomatic chronic active hepatitis. Hepatology 1 (5), 431–435.

Kobayashi, N., Fujiwara, T., Westerman, K.A., Inoue, Y., Sakaguchi, M., Noguchi, H., Miyazaki, M., Cai, J., Tanaka, N., Fox, I.J., Leboulch, P., 2000. Prevention of acute liver failure in rats with reversibly immortalized human hepatocytes. Science 287 (5456), 1258–1262.

Kremsdorf, D., Brezillon, N., 2007. New animal models for hepatitis C viral infection and pathogenesis studies. World J. Gastroenterol. 13 (17), 2427–2435.

Lerat, H., Honda, M., Beard, M.R., Loesch, K., Sun, J., Yang, Y., Okuda, M., Gosert, R., Xiao, S.Y., Weinman, S.A., Lemon, S.M., 2002. Steatosis and liver cancer in transgenic mice expressing the structural and nonstructural proteins of hepatitis C virus. Gastroenterology 122 (2), 352–365.

Moriya, K., Fujie, H., Shintani, Y., Yotsuyanagi, H., Tsutsumi, T., Ishibashi, K., Matsuura, Y., Kimura, S., Miyamura, T., Koike, K., 1998. The core protein of hepatitis C virus induces hepatocellular carcinoma in transgenic mice. Nat. Med. 4 (9), 1065–1067.

Moriya, K., Yotsuyanagi, H., Shintani, Y., Fujie, H., Ishibashi, K., Matsuura, Y., Miyamura, T., Koike, K., 1997. Hepatitis C virus core protein induces hepatic steatosis in transgenic mice. J. Gen. Virol. 78 (7), 1527–1531.

Nakai, M., Komiya, K., Murata, M., Kimura, T., Kanaoka, M., Kanegae, Y., Saito, I., 2007. Expression of pIX gene induced by transgene promoter: possible cause of host immune response in first-generation adenoviral vectors. Hum. Gene. Ther. 18 (10), 925–936.

Palmer, D.J., Ng, P., 2005. Helper-dependent adenoviral vectors for gene therapy. Hum. Gene. Ther. 16 (1), 1–16.

Shepard, C.W., Finelli, L., Alter, M.J., 2005. Global epidemiology of hepatitis C virus infection. Lancet Infect. Dis. 5 (9), 558–567.

Shintani, Y., Yotsuyanagi, H., Moriya, K., Fujie, H., Tsutsumi, T., Kanegae, Y., Kimura, S., Saito, I., Koike, K., 1999. Induction of apoptosis after switch-on of the hepatitis B virus X gene mediated by the Cre/loxP recombination system. J. Gen. Virol. 80 (12), 3257–3265.

Sun, J., Bodola, F., Fan, X., Irshad, H., Soong, L., Lemon, S.M., Chan, T.S., 2001. Hepatitis C virus core and envelope proteins do not suppress the host's ability to clear a hepatic viral infection. J. Virol. 75 (24), 11992–11998.

Sun, J., Tumurbaatar, B., Jia, J., Diao, H., Bodola, F., Lemon, S.M., Tang, W., Bowen, D.G., McCaughan, G.W., Bertolino, P., Chan, T.S., 2005. Parenchymal expression of CD86/B7.2 contributes to hepatitis C virus-related liver injury. J. Virol. 79 (16), 10730–10739.

Takaku, S., Nakagawa, Y., Shimizu, M., Norose, Y., Maruyama, I., Wakita, T., Takano, T., Kohara, M., Takahashi, H., 2003. Induction of hepatic injury by hepatitis C-virus-

specific CD8± murine cytotoxic T lymphocytes in transgenic mice expressing the viral structural genes. Biochem. Biophys. Res. Commun. 301, 330–337.
Takeuchi, T., Katsume, A., Tanaka, T., Abe, A., Inoue, K., Tsukiyama-Kohara, K., Kawaguchi, R., Tanaka, S., Kohara, M., 1999. Real-time detection system for quantification of hepatitis C virus genome. Gastroenterology 116 (3), 636–642.
Tumurbaatar, B., Sun, Y., Chan, T., Sun, J., 2007. Cre-estrogen receptor-mediated hepatitis C virus structural protein expression in mice. J. Virol. Methods 146 (1–2), 5–13.
Wakita, T., Katsume, A., Kato, J., Taya, C., Yonekawa, H., Kanegae, Y., Saito, I., Hayashi, Y., Koike, M., Miyamoto, M., Hiasa, Y., Kohara, M., 2000. Possible role of cytotoxic T cells in acute liver injury in hepatitis C virus cDNA transgenic mice mediated by Cre/loxP system. J. Med. Virol. 62 (3), 308–317.
Wakita, T., Taya, C., Katsume, A., Kato, J., Yonekawa, H., Kanegae, Y., Saito, I., Hayashi, Y., Koike, M., Kohara, M., 1998. Efficient conditional transgene expression in hepatitis C virus cDNA transgenic mice mediated by the Cre/loxP system. J. Biol. Chem. 273 (15), 9001–9006.
Yang, Y., Ertl, H.C., Wilson, J.M., 1994. MHC class I-restricted cytotoxic T lymphocytes to viral antigens destroy hepatocytes in mice infected with E1-deleted recombinant adenoviruses. Immunity 1 (5), 433–442.
Zhu, H.Z., Wang, W., Feng, D.M., Sai, Y., Xue, J.L., 2006. Conditional gene modification in mouse liver using hydrodynamic delivery of plasmid DNA encoding Cre recombinase. FEBS Lett. 580 (18), 4346–4352.

MAJOR ARTICLE

Monoclonal Antibody 2-152a Suppresses Hepatitis C Virus Infection Through Betaine/GABA Transporter-1

Masaaki Satoh,[1] Makoto Saito,[1] Takashi Takano,[1,2] Yuri Kasama,[1] Tomohiro Nishimura,[1,3] Yasumasa Nishito,[4] Yuichi Hirata,[2] Masaaki Arai,[2] Masayuki Sudoh,[5] Chieko Kai,[6] Michinori Kohara,[2] and Kyoko Tsukiyama-Kohara[1]

[1]Department of Experimental Phylaxiology, Faculty of Life Sciences, Kumamoto University, Honjo Kumamoto City; [2]Department of Microbiology and Cell Biology, Tokyo Metropolitan Institute of Medical Science, Kamikitazawa, Setagaya-ku; [3]KAKETSUKEN, Kyokushi, Kikuchi, Kumamoto; [4]Center for Microarray Analysis, Tokyo Metropolitan Institute of Medical Science; [5]Kamakura Research Laboratories, Chugai Pharmaceutical Co., Ltd., Kajiwara, Kamakura-City, Kanagawa; and [6]Laboratory of Animal Research Center, Institute of Medical Science, University of Tokyo, Shirokane-dai Minato-Ku, Japan

Background. We recently established a monoclonal antibody (2-152a MAb) that binds to 3β-hydroxysterol-Δ24-reductase (DHCR24) by immunizing mice with cells (RzM6-LC) persistently expressing hepatitis C virus (HCV). Here, we aimed to analyze the activity of 2-152a MAb against HCV replication and explore the molecular mechanism underlying the antiviral activity.

Methods. We characterized the effects of 2-152a MAb on HCV replication and performed a microarray analysis of antibody-treated HCV replicon cells. The molecules showing a significant change after the antibody treatment were screened to examine their relationship with HCV replication.

Results. The antibody had antiviral activity both in vitro and in vivo (chimeric mice). In the microarray analysis, 2-152a MAb significantly suppressed the expression of betaine/GABA transporter-1 (BGT-1) in 2 HCV replicon cell lines but not in HCV-cured cells. Silencing of BGT-1 expression by small interfering RNA (siRNA) revealed significant suppression of HCV replication and infection without cytotoxicity. Further, BGT-1 expression was significantly increased in the presence of HCV ($P < .05$).

Conclusions. Our results suggest that 2-152a MAb suppresses HCV replication and infection through BGT-1. These findings highlight important roles of BGT-1 in HCV replication and reveal a possible target for anti-HCV therapy.

Hepatitis C virus (HCV) causes chronic hepatitis and hepatocellular carcinoma (HCC) [1–3]. Chronic HCV infection is a major global public health concern because it affects at least 170 million people worldwide [2]. The most effective treatment against HCV currently comprises a combination therapy of PEGylated α-interferon (IFN-α) and ribavirin [4, 5]. However, considering that sustained virological responses develop in only approximately half of the patients infected with HCV genotype 1, the clinical efficacy of this therapy is limited [6, 7]. Efforts to develop therapies against HCV are further hindered by the high level of viral variation and capacity of the virus to cause chronic infection. Therefore, there is an urgent need to develop effective treatments against chronic HCV infection.

In a previous study, we established a cell line expressing HCV (RzM6-LC) to investigate the effects of persistent HCV expression on cell growth [8]. We also established a monoclonal antibody (2-152a MAb) against the RzM6-LC cell line to produce clones that recognize both cell surface and intracellular molecules. Using this method, we identified 3b-hydroxysterol-D24-reductase (DHCR24) as the recognition molecule of this antibody.

Received 30 November 2010; accepted 10 May 2011.

Correspondence: Kyoko Tsukiyama-Kohara, PhD, DVM, Department of Experimental Phylaxiology, Faculty of Life Sciences, Kumamoto University, 1-1-1 Honjo, Kumamoto-shi, Kumamoto 860-8556, Japan (kkohara@kumamoto-u.ac.jp).

The Journal of Infectious Diseases 2011;204:1172–80

0022-1899 (print)/1537-6613 (online)/2011/2048-0005$14.00
DOI: 10.1093/infdis/jir501

DHCR24 (also termed seladin-1) is an enzyme that catalyzes the conversion of desmosterol to cholesterol in the postsqualene cholesterol biosynthetic pathway [9, 10]. DHCR24 also acts as a hydrogen peroxide scavenger [11]. Therefore, DHCR24 may play a crucial role in maintaining cell physiology through cholesterol synthesis and oxidative stress. We previously demonstrated that HCV infection upregulates DHCR24 expression, and overexpression of DHCR24 inhibits apoptosis and inactivates the tumor suppressor gene p53 [12]. Moreover, silencing of DHCR24 suppressed HCV replication [13]. However, the precise mechanisms through which DHCR24 affects the HCV life cycle are unclear. In this study, we aimed to analyze the activity of 2-152a MAb against HCV replication and explore the molecular mechanism underlying the antiviral activity.

Materials And Methods

Cell Lines and Reagents

Human hepatoma cell line HuH-7 cell-based HCV replicon-harboring cell lines [14] R6FLR-N (genotype 1b) [15], FLR3-1 (genotype 1b) [16], and JFH-1 (genotype 2a) [17] were maintained in Dulbecco's modified Eagle's medium (DMEM) GlutaMAX (Invitrogen) containing 10% fetal calf serum (FCS; Sigma-Aldrich) in the presence of G418 (500 mg/mL for R6FLR-N and FLR3-1, 300 mg/mL for JFH-1; Invitrogen). Cured/HuH-7 histone H3 lysine 4 (K4) cells cured off HCV by interferon treatment [18] were maintained in DMEM GlutaMAX containing 10% FCS without G418. The JFH/K4 cell line persistently infected with the HCV JFH-1 strain and HuH-7 cell lines were maintained in DMEM containing 10% FCS [19]. The human hepatoblastoma HepG2 cell line was also maintained in DMEM containing 10% FCS.

Generation of 2-152a MAb

BALB/c strain of mice was immunized with 7–8 intraperitoneal injections of RzM6-LC cells (5×10^6) in RIBI adjuvant (trehalose dimycolate + monophosphoryl lipid A emulsion; RIBI ImmunoChem Research). After completion of the immunization regimen, their spleens were excised and splenocytes were fused with mouse myeloma plasminogen activator inhibitor (PAI) cells by using PEG1500 (Roche). Hybridoma cells were then selected with hypoxanthine, aminopterin, and thymidine (Invitrogen), and culture supernatants were collected for screening by whole-cell enzyme-linked immunosorbent assay (ELISA).

HCV Infection in Humanized Chimeric Mouse Liver and HCV mRNA Quantification by Real-time Detection Polymerase Chain Reaction

We purchased (from PhoenixBio Co.) chimeric mice that were established by transplanting human primary hepatocytes into severely combined immunodeficient (SCID) mice carrying a urokinase plasminogen activator (uPA) transgene controlled by an albumin promoter [20]. These mice were then infected with plasma isolated before 2003 from an HCV-positive patient (HCR6) [8, 21], in accordance with the Declaration of Helsinki. The protocols for the animal experiments were preapproved by the local ethics committee, and the animals were maintained in accordance with the National Institutes of Health Guide for the Care and Use of Laboratory Animals. HCV genotype 1b RNA levels were established at $0.96–1.84 \times 10^7$ copies/mL in mouse serum samples before the antibody treatment. The antibody (2-152a MAb) and normal immunoglobin G (IgG, 400 mg/20 g body weight) were intraperitoneally injected into the mice ($n = 4$) at 2-day intervals over a period of 14 days. IFN-α (30 mg/kg) was administered subcutaneously at 2-day intervals over a period of 2 weeks. Human serum albumin in the blood of chimeric mice was measured by using an Alb-II kit according to the manufacturer's instructions (Eiken Chemical). HCV RNA levels in serum and JFH/K4 cells were measured by real-time detection polymerase chain reaction (real-time detection [RTD]-PCR) as described previously [22]. HCV RNA in the cell cultures and supernatants was extracted by using Isogene and Isogene LS (Nippon Gene), respectively.

Replication Assay Using HCV Replicon Cells

We used 3 HCV subgenomic replicon cell lines: R6FLR-N, FLR3-1, and JFH-1. They were seeded at a density of 5×10^3 cells/well in 96-well tissue culture plates in DMEM GlutaMAX (Invitrogen) containing 5% fetal bovine serum (Thermo Scientific). Following incubation for 24 hours at 37°C (in 5% CO_2), the medium was removed and serial dilutions of antibody were added. Luciferase activity was determined by using a Bright-Glo luciferase assay kit (Promega) after 72 hours according to the manufacturer's instructions. The results were calculated as the average percentage relative to the reactivity in untreated cells, which was set at 100%. The viability of the replicon cells was measured by using a WST-8 cell counting kit (Dojindo) according to the manufacturer's instructions.

Immunostaining and Antibodies

Cells were cultured on glass coverslips (1.0 cm diameter) and fixed with 1% paraformaldehyde in phosphate-buffered saline (PBS) at room temperature for 10 minutes in 24-well plates. To permeabilize the cell membranes, the cells were treated with 1% Triton X-100 in PBS at room temperature for 10 minutes. After washing with 0.05% Tween-20 in PBS, the cells were incubated with 2-152a MAb, antiprotein disulfate isomerase (PDI) rabbit polyclonal antibody (Stressgen Bioreagents) or normal mouse IgG for 1 hour and washed with 0.05% Tween-20 in PBS. Alexa Fluor 488-labeled goat antimouse IgG was used as the secondary antibody.

Anti-NS5A antibody was provided by Dr Yoshiharu Matsuura (Osaka University). Anti-myc mouse monoclonal antibody

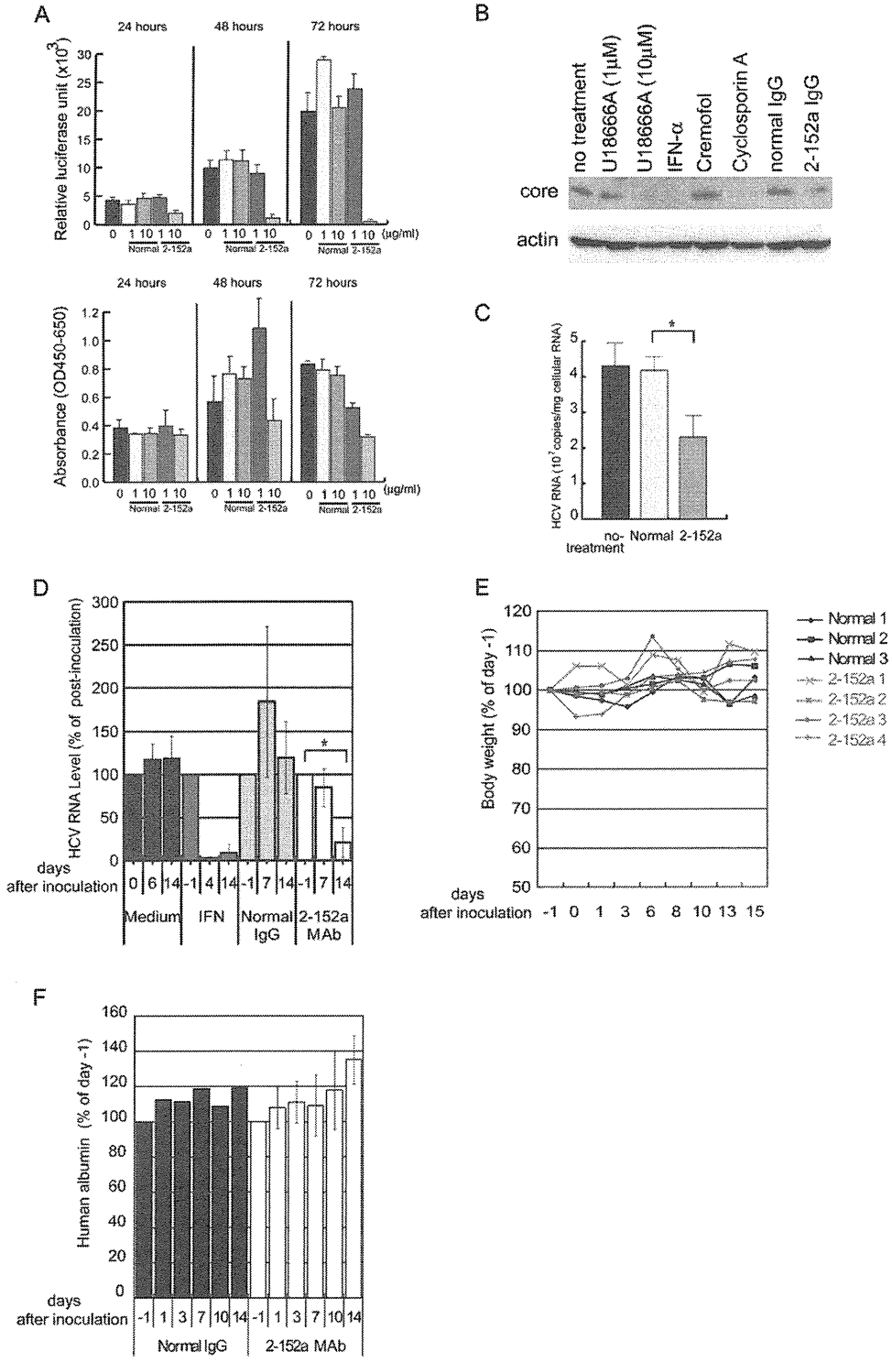

Figure 1. Anti-DHCR24 monoclonal antibody (2-152a MAb) suppresses HCV replication in vitro and in vivo. *A*, The effects of 2-152a MAb on HCV replication were measured by the luminescence activity and cell viability in FLR3-1 cells. The replicon cell line was incubated with IgG from normal mice or 2-152a MAb at 1 or 10 μg/mL for 24, 48, and 72 hours. The mean values from triplicate wells are indicated, and the vertical bars represent the standard deviation. The medium control (2% FCS-DMEM) without IgG is indicated as 0. *B*, The JFH/K4 cells were treated with cholesterol synthesis inhibitor U18666A (1 mM, 10 mM), IFN-α (250 IU/mL), Cyclosporin A (25 μM) and its solvent Cremophor, normal mouse IgG (10 μg/mL), and 2-152a IgG (10 μg/mL). HCV core and actin proteins were detected. *C*, HCV RNA copies were measured in JFH/K4 cells after treatment with normal or 2-152a IgG

(9E10; Cell Signaling Technology) and antiactin mouse monoclonal antibodies (Sigma-Aldrich) were utilized for detecting myc-fusion protein and normalization of the results, respectively.

cDNA Synthesis and Quantitative Reverse Transcriptase PCR

cDNA was synthesized from 0.5 or 1 mg of total RNA with a Superscript II kit (Invitrogen). TaqMan gene expression assays were custom designed and manufactured by Applied Biosystems. The expression was quantified with the ABI 7500 real-time PCR system (Applied Biosystems).

Microarray Analysis

For microarray analysis, total RNAs were extracted using RNAeasy kit (Qiagen), and RNA integrity was assessed using a Bioanalyzer (Agilent Technologies). cRNA targets were synthesized and hybridized with Whole Human Genome Oligo Microarray (G4112F; Agilent) according to the manufacturer's instructions.

RNA Interference, Expression Vector Construction, Transfection, and Rescue Experiments

Small interference RNA (siRNA) targeting betaine/GABA transporter-1 (BGT-1; nucleotides 120–144) was designed by using a program (https://rnaidesigner.invitrogen.com/) based on registered sequences in GenBank (5′-CAACAAGATGGAGT TTGTGCTGTCA-3′). Alternative siRNA (BGT-1-siRNA-362; nucleotides 362–386) was similarly designed. The HCV-siRNA (R7) sequence was 5′-GUCUCGUAGACCGUGCACCA dTdT-3′.

The coding region of the BGT-1 gene was obtained from RNA of R6FLR-N cells by reverse transcription–polymerase chain reaction (RT-PCR). The PCR products were inserted in *Eco*RV–*Xho*I sites of pcDNA6-myc His, version A (Invitrogen) after digestion of *Eco*RV–*Xho*I. To generate mutant plasmids that contained nucleotide substitutions in the siRNA-targeted site, we introduced point mutations into pcDNA-BGT-1 by using site-directed mutagenesis with a QuickChange multisite-directed mutagenesis kit (Stratagene), according to the manufacturer's instructions, and the following oligonucleotide primer: BGT-1-mut, 5′-CCAATGGACCAA-CAAGATGGAATTCGTTCTATCGGTGGCCGGGGAGCTC ATTGGG-3′ (the mutations introduced by mutagenesis are underlined).

Transfection of siRNAs was carried out by reverse transfection using Lipofectamine RNAiMAX according to the manufacturer's protocol (Invitrogen). Transfection of the expression vector was undertaken by using Lipofectamine LTX with Plus reagent (Invitrogen).

The rescue experiment was performed after reverse transfection of BGT-1 siRNA (1.5 nM) into R6FLR-N cells by using RNAiMAX reagent. After 48 hours, wild-type (wt) and mutant (mut) BGT-1 expression vectors (10 ng) were transfected by using Lipofectamine LTX, and the luciferase activity and cell viability were assessed by WST-8 assay (Dojindo) after 24 hours.

Analysis of HCV Infection and BGT-1 Expression

For infection assays, Cured/HuH-7 K4 cells were incubated with JFH/K4 cell-derived HCV (2.0×10^6 copies/mL). At 72 hours after incubation, HCV infection and BGT-1 expression were analyzed by real-time detection (RTD)-PCR and TaqMan expression assay, respectively, as described earlier.

Statistical Analysis

The Student t test was used to test the statistical significance of the results. P values $< .05$ were considered statistically significant.

Results

Inhibitory Effect of 2-152a MAb on HCV Replication In Vitro

We examined the effects of 2-152a MAb on HCV replication and the viability in HCV replicon cell lines. The treatment with 2-152a MAb significantly decreased HCV replication after 48 hours and cell viability after 72 hours (Figure 1*A*). To determine the recognition site of 2-152a MAb, we performed epitope mapping by using serial overlapping deletion mutants of the DHCR24 fusion protein (Supplementary Figure 1*A*). The recognition site was identified within amino acid residues 259–314 (Supplementary Figure 1*B*) and the predicted "Diminuto-like protein" homologous region [23] indicated in Supplementary Figure 1A.

Suppression of HCV Infection by 2-152a MAb

To determine the effects of 2-152a MAb on HCV infection, we inoculated the antibody into a persistently HCV-infected cell line (JFH/K4; Figure 1*B* and *C*) or uPA-SCID chimeric mice previously transplanted with human hepatocytes [20] and

Figure 1 continued. (10 μg/mL). The error bars indicate the standard deviation, and the asterisk indicates $P < .005$. *D*, Relative amounts of HCV RNA (% copies/mg total RNA on days −1 or 0) in the livers of chimeric mice inoculated with the control medium, PEGylated IFN-α, normal IgG, or 2-152a IgG were estimated by RTD-PCR. For normalization, the HCV RNA level 1 day before the inoculation (day −1) or on the day of inoculation (day 0) was defined as 100%. The graph shows the relative amounts of HCV RNA at −1 day (or day 0), 7 days (or 4 days), and 14 days. The error bars indicate the standard deviation, and the asterisk indicates $P < .005$. *E*, Ratio of body weight of mice inoculated with either normal IgG or 2-152a MAb IgG to that on day −1. *F*, Ratio of albumin concentration in serum samples of mice inoculated with 2-152a MAb IgG or normal IgG to that on day −1. The vertical bars indicate the standard deviation.

A

R6 2-152a 24h Gene Name	2-152a/normal IgG	FLR3-1 2-152a 24h Gene Name	2-152a/normal IgG	FLR3-1 2-152a 72h Gene Name	2-152a/normal IgG	K4 2-152a 24h Gene Name	2-152a/normal IgG
CNN1	2.63	CNN1	2.18	CGA	1.54	KIAA0367	1.97
A_24_P3983 70	2.57	ACTA1	1.98	TAGLN	1.47	ACTA1	1.90
ACTA1	2.44	SLC16A14	1.59	CNN1	1.39	CNN1	1.88
CSTA	1.71	TAGLN	1.52			A_24_P398370	1.81
ENST000002 98047	1.7	LYPD1	1.51	RSNL2	0.75	SLC16A14	1.80
TAGLN	1.63	IL11	1.51	SLC37A2	0.74	ADH1A	1.59
AI379175	1.6	KCNJ8	1.41	AKR1C1	0.73	ROBO2	1.56
MGAM	1.58	MSRB3	1.4	BG542103	0.72	AKR1D1	1.54
MSRB3	1.57	C8orf4	1.4	PTGS1	0.71	SLC17A1	1.50
MSRB3	1.56	PPP3R1	1.39	THC2437143	0.71	SLC16A14	1.47
EPPK1	1.47	ELF5	0.73	AKR1B10	0.71	BC036599	1.46
THC2317432	1.45	CYP3A7	0.72	SLC6A14	0.70	TAGLN	1.44
AK055214	1.43	COL14A1	0.71	AKR1B10	0.70	MSRB3	1.43
SLC16A6	1.39	LOC401022	0.71	COL14A1	0.69	SOCS2	1.37
AKR1C1	0.75	THC2437143	0.7	SLC6A14	0.69	FXYD2	0.74
AKR1C1	0.74	BG542103	0.7	SMPD3	0.67	ENST00000036	0.73
CD44	0.74	S100A4	0.7	VNN2	0.66	SLC7A6	0.72
CD44	0.73	PTGS1	0.69	FXYD2	0.65	ARG2	0.72
ARG1	0.72	F2RL2	0.68	F2RL2	0.62	IGFBP5	0.71
F2RL2	0.72	FUT5	0.67	BGT-1	0.61	ROBO3	0.71
CYP3A7	0.71	FCGBP	0.66	FXYD2	0.59	GPX2	0.70
CD44	0.7	FUT3	0.64	FLJ25422	0.42	CR603668	0.70
LOC642775	0.7	PTGS1	0.64			IGFBP6	0.69
S100A4	0.68	SLC6A14	0.63			COL14A1	0.69
SLC7A6	0.67	VNN2	0.63			AF116081	0.68
VNN2	0.65	THC2442210	0.63			VNN2	0.67
ROBO3	0.65	ZNF114	0.62			HOXD1	0.66
CDKN1C	0.63	SMPD3	0.61			CDKN1C	0.66
FUT3	0.61	BGT-1	0.58			THC2442210	0.66
KCNMA1	0.6	CDKN1C	0.49			LOC647022	0.65
BGT-1	0.58					COL14A1	0.62
						SLC6A14	0.53
						FUT3	0.53

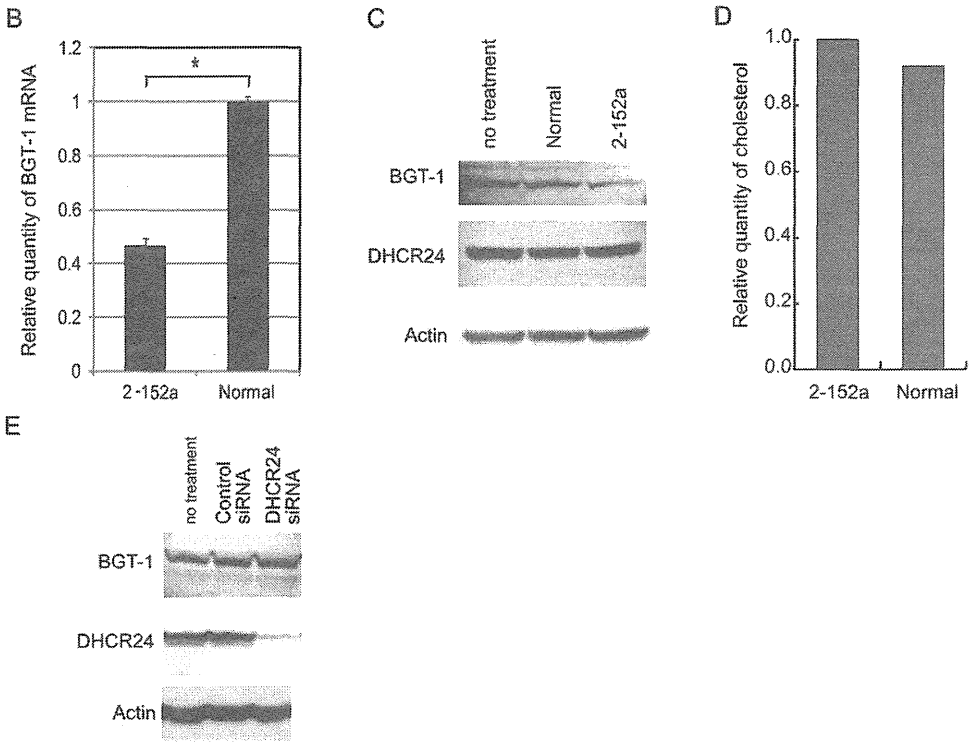

Figure 2. *A*, Genes that showed significant changes in expression after the 2-152a MAb treatment. HCV replicon cells (FLR3-1 and R6FLR-N) and K4 cells were treated with 2-152a MAb. The symbols shaded in gray indicate the genes that showed significantly changed expression commonly in R6FLR-N and FLR3-1 cells, and those shaded in orange indicate the genes that showed significantly changed expression in K4 cells. The amount of labeled probe for microarray analysis was 7-fold higher than that in the first experiment (Supplementary Table 1). Each value indicates the number of ratios of signal 2-152a MAb/normal IgG treatment. *B*, TaqMan expression assay of BGT-1 in samples of R6FLR-N cells treated with 2-152a MAb or normal IgG. BGT-1 mRNA (0.5 μg) samples treated with 2-152a MAb or normal IgG were transcribed by reverse transcriptase, and synthesized cDNAs were used for TaqMan

infected with HCV (Figure 1*D* and *F*). We detected viral protein (core) (Figure 1*B*) or viral RNA in cells (Figure 1*C*) and mouse blood by using RTD-PCR (Figure 1*D*). There was a significant reduction in the viral titers with 2-152a MAb treatment compared with that in normal IgG treatment (control) ($P < .005$, Figure 1*C* and *D*). No significant effects on body weight were observed by the inoculation of 2-152a MAb (Figure 1*E*). Further, no significant differences were found among the levels of human albumin in the sera of the normal IgG- and 2-152a MAb-inoculated mice (Figure 1*F*).

Expression of DHCR24 in Carcinoma Cells and on the Surface of HuH-7-Derived Cells

We observed abundant intracellular expression of DHCR24 in hepatoma cell lines in the previous study [12]; therefore, we characterized its expression on the surface of various carcinoma cell lines by flow cytometric analysis to clarify the mechanism of 2-152a MAb antiviral effects. In this analysis, DHCR24 expression was localized to the surface of the HuH-7 and HuH-7-based cell lines, HCV replicon cell lines (R6FLR-N, FLR3-1, and JFH-1), HCV persistently infected cell line (JFH/K4), and K4 cells; on the other hand, DHCR24 was not significantly expressed on the surface of the HepG2, Hep3B, RzM6-0d, RzM6-LC, WRL68, and PLC/PRF/5 cell lines (Supplementary Figure 1*C*). To confirm the expression of DHCR24 on the cell surface, we performed immunofluorescence staining (Supplementary Figure 1*D*). DHCR24 expression was detected in the HuH-7 cells without permeabilization.

Suppression of BGT-1 mRNA Expression in HCV Replicon Cell Lines After Treatment With 2-152a MAb

To determine the molecular mechanism underlying the effects of 2-152a MAb, we performed microarray analysis twice with different amounts of probes and evaluated the changes in gene expression associated with the 2-152a MAb treatment, which were specific to the HCV replicon cells rather than to the HCV-cured K4 cells. Using this methodology, we identified approximately 3–14 genes as upregulated and about 17–20 genes as downregulated following the treatment with 2-152a MAb, compared with the expressions in normal IgG-treated R6FLR-N, FLR3-1, and K4 cells (Figure 2*A*). Among these genes, the expression level of SLC6A12 (BGT-1; GenBank accession number NM_003044) showed significant downregulation in both the R6FLR-N and the FLR3-1 cell lines but not in the K4 cells (Figure 2*A*; Table 1). To validate this result, we tested BGT-1 mRNA expression in R6FLR-N cells treated with 2-152a MAb and normal IgG by using TaqMan expression assay. This assay demonstrated that the relative expression of BGT-1 was significantly suppressed by the treatment with 2-152a MAb ($P < .001$, Figure 2*B*). Significant downregulation of BGT-1 was also observed by treatment with 2-152a MAb in HCV-JFH-1-infected cells (Figure 2*C*).

Table 1. Screened Genes in HCV Replicon Cell Lines After Treatment of IgG

	Gene name	R6FLR-N 24 hours	FLR3-1 24 hours	FLR3-1 72 hours	HuH-7/K4 24 hours
Screened specifically in replicon cells[a]					
1st screening	AKR1C1	0.67	0.62	0.65	NS
	BGT-1	0.53	0.63	0.53	NS
2nd screening (7-fold)[a]	AKR1C1	0.74 or 0.75	NS	0.73	NS
	F2RL2	0.72	0.68	0.62	NS
	BGT-1	0.58	0.58	0.61	NS
Screened in replicon and cured K4 cells[b]					
1st screening	CNN1	2.75	0.6	1.62	1.9
2nd screening (7-fold)[c]	CNN1	2.63	2.18	1.39	1.88
	TAGLN	1.63	1.52	1.47	1.44
	VNN2	0.65	0.63	0.66	0.67

Abbreviations: HCV, hepatitis C virus; IgG, immunoglobin G; NS, not screened.

[a] Screened genes were significantly changed in HCV replicon cells but not in HuH-7/K4 cells; each value indicates ratio of signal 2-152a MAb IgG/normal IgG treatment.

[b] Screened genes were significantly changed in all cell lines, including replicon cells and HuH-7/K4 cells.

[c] Comparing to 1st screening, 7-fold amount of labeled probe was used for microarray.

We further addressed the mechanism of action of 2-152a MAb. Treatment with 2-152a MAb did not decrease the level of cholesterol (Figure 2*D*), and silencing of DHCR24 did not influence BGT-1 significantly (Figure 2*E*).

Inhibition of HCV Replication and Infection by siRNA Directed Against BGT-1

Because BGT-1 expression was suppressed by the treatment with 2-152a MAb, which had antiviral activity, we attempted BGT-1 silencing in HCV replicon cell lines by using designed siRNAs to examine the potential role of BGT-1 in HCV replication. BGT-1 silencing was confirmed by RT-PCR (Figure 3*A*). The effect of the siRNAs on HCV replication was examined by Western blotting with anti-NS5A antibody (Figure 3*B*) and measured by the luminescence level (Figure 3*C*, left panel) and cell viability (Figure 3*C*, right panel) in FLR3-1 cells. We also examined the effect of these siRNAs in R6FLR-N and JFH-1 cells (Supplementary Figure 2*A*) and observed similar inhibitory effects as

Figure 2 continued. gene expression assay. Each value was compensated with values of glyceraldehyde 3-phosphate dehydrogenase (GAPDH) mRNA as the internal control and normal IgG. The asterisk indicates $P < .001$, and the vertical bars indicate the standard deviation. *C*, Level of BGT-1 and DHCR24 proteins detected in JFH/K4 cells after treatment with 2-152a or normal IgG (10 μg/mL). *D*, The relative cholesterol amount was measured in R6FLR-N cells treated with 2-152a or normal IgG (10 μg/mL). *E*, BGT-1 and DHCR24 proteins were detected in normal IgG- or 2-152a IgG-treated R6FLR-N cells.

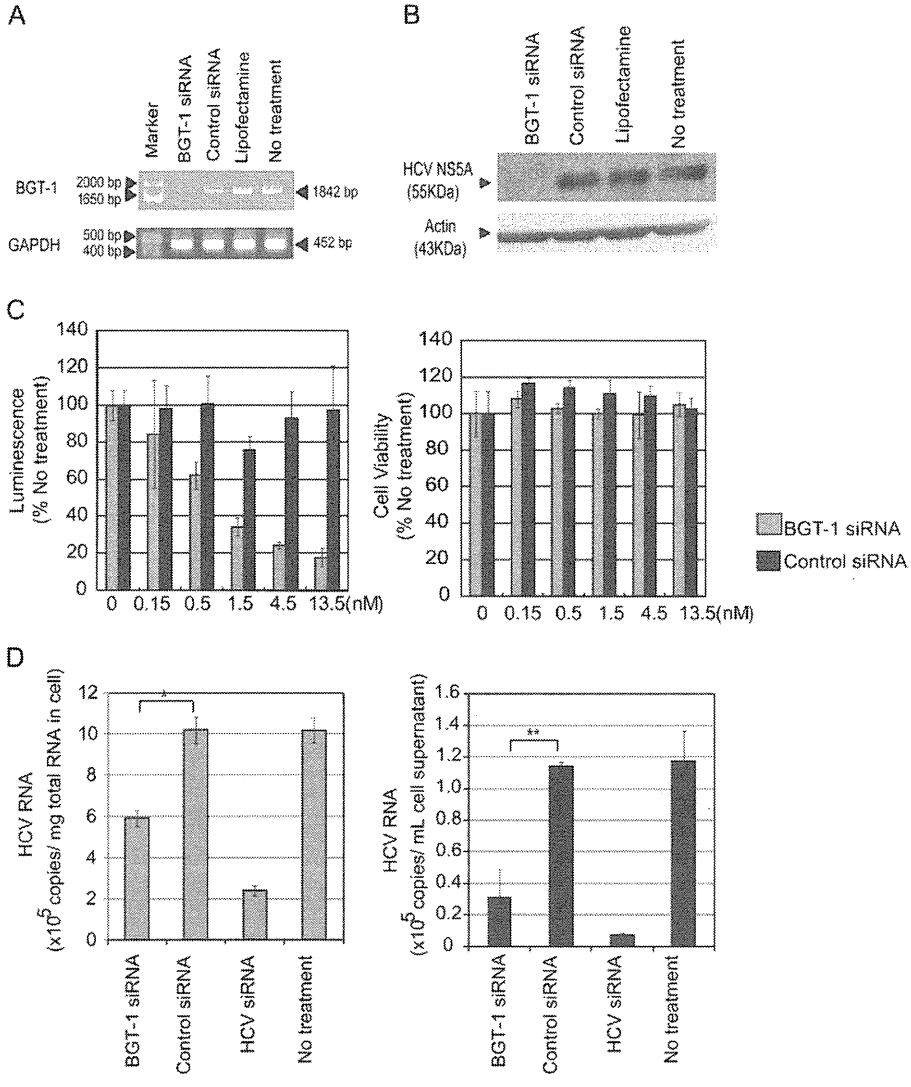

Figure 3. BGT-1 silencing by siRNA inhibits HCV replication in subgenomic HCV replicon cell lines and the persistently infected cell line. *A*, The siRNA targeting BGT-1 suppressed the expression of the corresponding mRNA. The mRNA of each sample was extracted 72 hours after siRNA (10 nM) transfection. Total RNA was transcribed and amplified by RT-PCR using primers specific to the open reading frame (ORF) of the BGT-1 (1842 bp) gene. The experiments were performed in triplicate, and the representative data are presented. *B*, The effects of BGT-1 siRNA (10 nM) on HCV were confirmed by Western blot analysis using an antibody against the HCV NS5A protein (55 kDa). The blots were striped and reprobed with an antibody directed against actin to examine protein loading in each lane. *C*, Levels of HCV replication (left panel) and cell viability (right panel) are presented according to serial concentrations of siRNA targeting BGT-1 and control siRNA in FLR3-1 cells (72 hours after transfection). The inhibition of replication or cell viability following siRNA targeting BGT-1 is defined relative to those of the cells that received no treatment (100%). The error bars represent the standard error of triplicate experiments. *D*, Quantification of HCV RNA by RTD-PCR in HCV persistently infected cells (JFH/K4) after treatment with BGT-1 siRNA. The cells were treated with siRNAs (10 nM) against BGT-1, control, and HCV (HCV R7) and harvested at 72 hours after transfection. TaqMan quantitative RT-PCR was performed for quantitation of HCV RNA in extracted RNA from cells (left panel) and their supernatants (right panel). The single asterisk (*) and double asterisk (**) indicate $P < .005$ and $P < .05$ against the control, respectively. The mean values from triplicate wells are indicated, and the vertical bars indicate the standard deviation.

those in FLR3-1 cells. The median inhibitory concentration (IC_{50}) values of BGT-1 siRNAs in various HCV replicon cell lines were as follows: FLR3-1 cells, 0.93 nM; R6FLR-N cells, 1.37 nM; JFH-1 cells, 5.95 nM. The cell viability was not significantly influenced by the siRNA treatment (Figure 3*C*, right panel; Supplementary Figure 2*A*, right panel).

Further, we monitored the levels of HCV RNA in JFH/K4 cells and their supernatants after BGT-1 silencing. Using RTD-PCR, we detected significant suppression in the HCV RNA levels by BGT-1 silencing in these cells ($P < .005$; Figure 3*D*, left panel) and their supernatants ($P < .05$; Figure 3*D*, right panel). These results were consistent with the strong inhibitory effects of

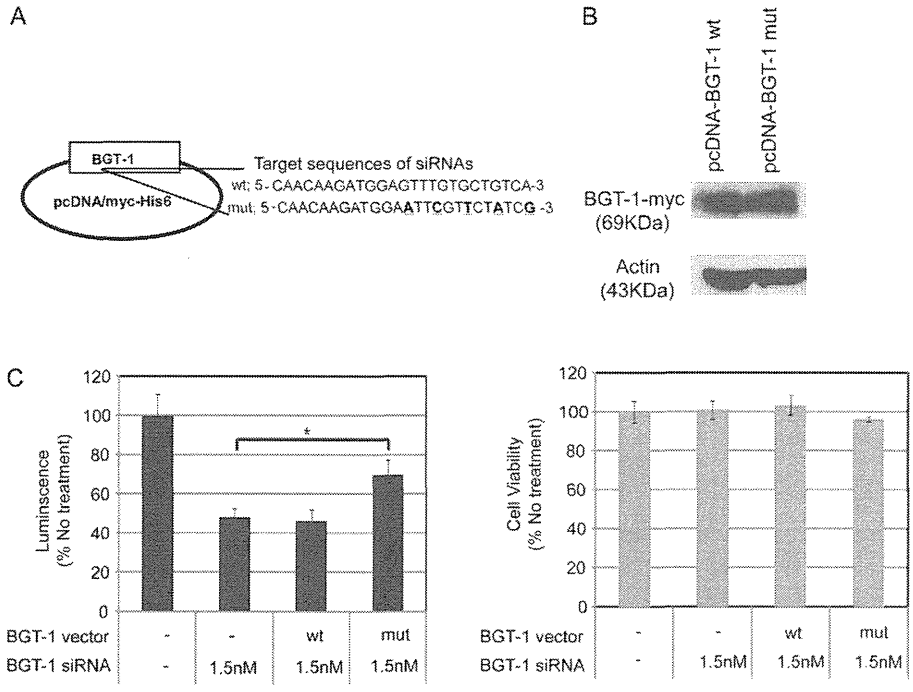

Figure 4. Validation of the inhibitory effects of BGT-1 siRNA on HCV replication in subgenomic HCV replicon cell lines. *A*, Schematic representation of the pcDNA-BGT-1 wild-type (wt) and mutant (mut) plasmids. The siRNA-targeted sites are indicated, and the underlined bold letters indicate the sequences induced by mutagenesis PCR. *B*, The wild type and mutant of the BGT-1-myc fusion protein were detected by using an anti-myc monoclonal antibody (9E10) in transfected R6FLR-N cells (upper panel). The blots were striped and reprobed with an antibody against actin to determine protein loading for each lane (lower panel). *C*, R6FLR-N cells were transfected with BGT-1 siRNA, and wild-type or mutant expression vectors were transfected after siRNA transfection. After 24 hours of vector transfection, the level of HCV replication (left panel) was measured by luminescence, and cell viability (right panel) was measured by WST-8 assay. The asterisk indicates $P < .05$ compared with transfection of siRNA alone. The mean values from triplicate wells are indicated, and the vertical bars represent the standard deviation.

BGT-1 siRNA on HCV replication, as shown in Figure 3*C*. We designed alternative siRNA targeting BGT-1 (BGT-1-siRNA-362) and observed its significant inhibitory effect on HCV replication without significant cytotoxicity (Supplementary Figure 2*B*).

Validation of the Anti-HCV Effects of siRNA Against BGT-1 by Rescue With Expression Vectors

To assess the specificity of BGT-1 silencing, we attempted to rescue HCV replication against the ectopic effects by this silencing. To examine the effect of the rescue, we constructed expression vectors of wild-type and mutant BGT-1 (Figure 4*A*) and confirmed the expression of each BGT-1-myc-fused protein (Figure 4*B*). The mutant BGT-1 vector contained 5 base mismatches within the site targeted by the BGT-1 siRNA without a change in the amino acid sequence of the protein (underlined in Figure 4*A*). We also transfected the pcDNA-BGT-1 plasmid after the siRNA treatment and observed significant recovery of HCV replication with mutant pcDNA-BGT-1 ($P < .05$; Figure 4*C*, left panel) without significant cytotoxicity (Figure 4*C*, right panel). BGT-1 expression was increased significantly in K4 cells in the presence of HCV ($P < .05$, Supplementary Figure 2*C*) at 72 hours after infection compared with the absence of HCV, and in RzM6-LC cells, which persistently express HCV [8], compared with RzM6-0d cells, which lack HCV expression ($P < .05$, Supplementary Figure 2*D*).

DISCUSSION

In this study, we determined that 2-152a MAb, which binds to but does not affect the activity of DHCR24, suppresses HCV replication and that BGT-1 is highly downregulated in HCV replicon cell lines treated with this antibody. Further, the efficient rescue of viral replication with a mutant expression vector indicates the specific inhibitory effect of BGT-1 silencing on HCV replication. Therefore, we hypothesize that BGT-1 plays an important role in HCV replication through a pathway that is likely independent of DHCR24, which in its own right can regulate the HCV life cycle [13].

BGT-1 is involved in sodium- and chloride-coupled betaine uptake, which helps in maintaining normal cellular conditions. Previous reports have described that the transcription of BGT-1 mRNA is regulated by a tonicity sensitive element (TonE) in response to hypertonic stress, a result that was first identified in the Madin-Darby canine kidney (MDCK) cell line [24]. BGT-1

is also thought to be responsible for the hyperosmotic stress response and in maintaining cell hydration. Denkert et al [25] reported that BGT-1 gene expression is induced by hyperosmolarity and inhibited by p38 mitogen-activated protein kinase ($p38^{MAPK}$) inhibitor SB20358. Further, several reports have evidenced that cell hydration affects viral replication and that viral replication increases during cell shrinkage due to hyperosmolarity, a result that was accompanied by increased BGT-1 mRNA expression [26]. Considering the reduction in HCV replication by the BGT-1 siRNA treatment, this treatment may prevent HCV replication by affecting hypoosmotic conditions in HCV-infected cells. Further studies are required to examine in detail the function of BGT-1 in HCV replication.

In summary, we demonstrated that the 2-152a monoclonal antibody inhibits HCV replication in HCV replicon cells and HCV infection in human hepatocytes transplanted into chimeric mice. The inhibitory effect of the monoclonal antibody on viral replication may be mediated by the suppression of BGT-1 expression. We propose BGT-1 as a key target for anti-HCV therapies.

Supplementary Data

Supplementary materials are available at *The Journal of Infectious Diseases* online (Supplementary Data).

Supplementary materials consist of data provided by the author that are published to benefit the reader. The posted materials are not copyedited. The contents of all supplementary data are the sole responsibility of the authors. Questions or messages regarding errors should be addressed to the author.

Notes

Acknowledgments. The authors thank I. Maruyama, K. Tanaka, T. Seki, and R. Takehara for their excellent technical support, and Y. Tokunaga for the insightful comments and helpful discussion.

Financial Support. This work was supported by grants from the Ministry of Health and Welfare of Japan; Ministry of Education, Culture, Sports, Science and Technology of Japan; Program for Promotion of Fundamental Studies in Health Sciences of the National Institute of Biomedical Innovation; and Cooperative Research Project on Clinical and Epidemiological Studies of Emerging and Reemerging Infectious Diseases.

Potential conflicts of interest. All authors: No reported conflicts.

All authors have submitted the ICMJE Form for Disclosure of Potential Conflicts of Interest. Conflicts that the editors consider relevant to the content of the manuscript have been disclosed.

References

1. Di Bisceglie AM, Carithers RL Jr, Gores GJ. Hepatocellular carcinoma. Hepatology **1998**; 28:1161–5.
2. Hayashi J, Aoki H, Arakawa Y, Hino O. Hepatitis C virus and hepatocarcinogenesis. Intervirology **1999**; 42:205–10.
3. Michielsen PP, Francque SM, van Dongen JL. Viral hepatitis and hepatocellular carcinoma. World J Surg Oncol **2005**; 3:27.
4. Mazzella G, Accogli E, Sottili S, et al. Alpha interferon treatment may prevent hepatocellular carcinoma in HCV-related liver cirrhosis. J Hepatol **1996**; 24:141–7.
5. Bruchfeld A, Stahle L, Andersson J, Schvarcz R. Ribavirin treatment in dialysis patients with chronic hepatitis C virus infection—a pilot study. J Viral Hepat **2001**; 8:287–92.
6. Kohara M, Tanaka T, Tsukiyama-Kohara K, et al. Hepatitis C virus genotypes 1 and 2 respond to interferon-alpha with different virologic kinetics. J Infect Dis **1995**; 172:934–8.
7. Nakamura H, Ogawa H, Kuroda T, et al. Interferon treatment for patients with chronic hepatitis C infected with high viral load of genotype 2 virus. Hepatogastroenterology **2002**; 49:1373–6.
8. Tsukiyama-Kohara K, Toné S, Maruyama I, et al. Activation of the CKI-CDK-Rb-E2F pathway in full genome hepatitis C virus-expressing cells. J Biol Chem **2004**; 279:14531–41.
9. Crameri A, Biondi E, Kuehnle K, et al. The role of seladin-1/DHCR24 in cholesterol biosynthesis, APP processing and Aβ generation in vivo. EMBO J **2006**; 25:432–43.
10. Waterham HR, Koster J, Romeijn GJ, et al. Mutations in the 3β-hydroxysterol Δ^{24}-reductase gene cause desmosterolosis, an autosomal recessive disorder of cholesterol biosynthesis. Am J Hum Genet **2001**; 69:685–94.
11. Lu X, Kambe F, Cao X, et al. 3β-Hydroxysteroid-Δ24 reductase is a hydrogen peroxide scavenger, protecting cells from oxidative stress-induced apoptosis. Endocrinology **2008**; 149:3267–73.
12. Nishimura T, Kohara M, Izumi K, et al. Hepatitis C virus impairs p53 via persistent overexpression of 3β-hydroxysterol Δ24-reductase. J Biol Chem **2009**; 284:36442–52.
13. Takano T, Tsukiyama-Kohara K, Hayashi M, et al. Augmentation of DHCR24 expression by hepatitis C virus infection facilitates viral replication in hepatocytes. J Hepatol **2011**; 55:512–21.
14. Lohmann V, Körner F, Koch J, Herian U, Theilmann L, Bartenschlager R. Replication of subgenomic hepatitis C virus RNAs in a hepatoma cell line. Science **1999**; 285:110–3.
15. Watanabe T, Sudoh M, Miyagishi M, et al. Intracellular-diced dsRNA has enhanced efficacy for silencing HCV RNA and overcomes variation in the viral genotype. Gene Ther **2006**; 13:883–92.
16. Sakamoto H, Okamoto K, Aoki M, et al. Host sphingolipid biosynthesis as a target for hepatitis C virus therapy. Nat Chem Biol **2005**; 1:333–7.
17. Kato T, Date T, Miyamoto M, et al. Efficient replication of the genotype 2a hepatitis C virus subgenomic replicon. Gastroenterology **2003**; 125: 1808–17.
18. Blight KJ, McKeating JA, Rice CM. Highly permissive cell lines for subgenomic and genomic hepatitis C virus RNA replication. J Virol **2002**; 76:13001–14.
19. Wakita T, Pietschmann T, Kato T, et al. Production of infectious hepatitis C virus in tissue culture from a cloned viral genome. Nat Med **2005**; 11:791–6.
20. Mercer DF, Schiller DE, Elliott JF, et al. Hepatitis C virus replication in mice with chimeric human livers. Nat Med **2001**; 7:927–33.
21. Inoue K, Umehara T, Ruegg UT, et al. Evaluation of a cyclophilin inhibitor in hepatitis C virus-infected chimeric mice in vivo. Hepatology **2007**; 45:921–8.
22. Takeuchi T, Katsume A, Tanaka T, et al. Real-time detection system for quantification of hepatitis C virus genome. Gastroenterology **1999**; 116:636–42.
23. Sarkar D, Imai T, Kambe F, et al. The human homolog of Diminuto/Dwarf1 gene (hDiminuto): a novel ACTH-responsive gene overexpressed in benign cortisol-producing adrenocortical adenomas. J Clin Endocrinol Metab **2001**; 86:5130–7.
24. Takenaka M, Preston AS, Kwon HM, Handler JS. The tonicity-sensitive element that mediates increased transcription of the betaine transporter gene in response to hypertonic stress. J Biol Chem **1994**; 269: 29379–81.
25. Denkert C, Warskulat U, Hensel F, Häussinger D. Osmolyte strategy in human monocytes and macrophages: involvement of p38MAPK in hyperosmotic induction of betaine and myoinositol transporters. Arch Biochem Biophys **1998**; 354:172–80.
26. Häussinger D. The role of cellular hydration in the regulation of cell function. Biochem J **1996**; 313:697–710.

Herpes simplex encephalitis in children with autosomal recessive and dominant TRIF deficiency

Vanessa Sancho-Shimizu,[1,2] Rebeca Pérez de Diego,[1,2] Lazaro Lorenzo,[1,2] Rabih Halwani,[3] Abdullah Alangari,[3] Elisabeth Israelsson,[4] Sylvie Fabrega,[5] Annabelle Cardon,[1,2] Jerome Maluenda,[1,2] Megumi Tatematsu,[6] Farhad Mahvelati,[7] Melina Herman,[8] Michael Ciancanelli,[8] Yiqi Guo,[8] Zobaida AlSum,[3] Nouf Alkhamis,[3] Abdulkarim S. Al-Makadma,[9] Ata Ghadiri,[10,11] Soraya Boucherit,[1,2] Sabine Plancoulaine,[1,2] Capucine Picard,[1,2,12,13] Flore Rozenberg,[14] Marc Tardieu,[15] Pierre Lebon,[14] Emmanuelle Jouanguy,[1,2,13] Nima Rezaei,[16,17] Tsukasa Seya,[6] Misako Matsumoto,[6] Damien Chaussabel,[4] Anne Puel,[1,2] Shen-Ying Zhang,[1,8] Laurent Abel,[1,2,8] Saleh Al-Muhsen,[3] and Jean-Laurent Casanova[1,2,3,8,12]

[1]Laboratory of Human Genetics of Infectious Diseases, Necker Branch, Institut National de la Santé et de la Recherche Médicale, Necker Medical School, Paris, France. [2]University Paris Descartes, Paris, France. [3]Prince Naif Center for Immunology Research, Department of Pediatrics, College of Medicine, King Saud University, Riyadh, Saudi Arabia. [4]Benaroya Research Institute at Virginia Mason, Seattle, Washington, USA. [5]Viral Vector and Gene Transfer Platform, University Paris Descartes, Institut Fédératif de Recherche Necker Enfants Malades, Paris, France. [6]Department of Microbiology and Immunology, Hokkaido University Graduate School of Medicine, Sapporo, Japan. [7]Child Neurology Department, Mofid Children Hospital, Shahid Beheshti University of Medical Sciences, Tehran, Iran. [8]Laboratory of Human Genetics of Infectious Diseases, Rockefeller Branch, The Rockefeller University, New York, New York, USA. [9]King Fahd Medical City, Riyadh, Saudi Arabia. [10]Department of AIDS and Hepatitis, Pasteur Institute, Tehran, Iran. [11]Department of Immunology, Faculty of Medicine, Ahvaz Jundishapur University of Medical Sciences, Ahvaz, Iran. [12]Pediatric Hematology-Immunology Unit and [13]Study Center of Primary Immunodeficiencies, Necker Hospital, Paris, France. [14]Virology, Cochin Hospital, University Paris Descartes, Paris, France. [15]Pediatric Neurology, Bicêtre Hospital, University Paris Sud, Kremlin-Bicêtre, France. [16]Research Center for Immunodeficiencies, Pediatrics Center of Excellence, Children's Medical Center, and [17]Molecular Immunology Research Center and Department of Immunology, School of Medicine, Tehran University of Medical Sciences, Tehran, Iran.

Herpes simplex encephalitis (HSE) is the most common sporadic viral encephalitis of childhood. Autosomal recessive (AR) UNC-93B and TLR3 deficiencies and autosomal dominant (AD) TLR3 and TRAF3 deficiencies underlie HSE in some children. We report here unrelated HSE children with AR or AD TRIF deficiency. The AR form of the disease was found to be due to a homozygous nonsense mutation that resulted in a complete absence of the TRIF protein. Both the TLR3- and the TRIF-dependent TLR4 signaling pathways were abolished. The AD form of disease was found to be due to a heterozygous missense mutation, resulting in a dysfunctional protein. In this form of the disease, the TLR3 signaling pathway was impaired, whereas the TRIF-dependent TLR4 pathway was unaffected. Both patients, however, showed reduced capacity to respond to stimulation of the DExD/H-box helicases pathway. To date, the TRIF-deficient patients with HSE described herein have suffered from no other infections. Moreover, as observed in patients with other genetic etiologies of HSE, clinical penetrance was found to be incomplete, as some HSV-1–infected TRIF-deficient relatives have not developed HSE. Our results provide what we believe to be the first description of human TRIF deficiency and a new genetic etiology for HSE. They suggest that the TRIF-dependent TLR4 and DExD/H-box helicase pathways are largely redundant in host defense. They further demonstrate the importance of TRIF for the TLR3-dependent production of antiviral IFNs in the CNS during primary infection with HSV-1 in childhood.

Introduction

Herpes simplex encephalitis (HSE) is a rare and potentially fatal manifestation of herpes simplex virus-1 (HSV-1) infection, with an incidence of about 1 in 250,000 individuals per year (1). With the introduction of acyclovir from the 1980s onward, HSE mortality rates, which used to be as high as 70%, have declined significantly (2, 3), although most patients, affected children in particular, continue to suffer life-long neurological sequelae (4–6). The incidence of HSE peaks between the ages of 6 months and 3 years, a period during which the vast majority of cases are a consequence of primary infection with HSV-1 (7–9). The pathogenesis of HSE, first described in 1941, remained elusive until the demonstration of an underlying role in this devastating disease, in at least some children, of autosomal recessive (AR) UNC-93B deficiency in 2006, autosomal dominant (AD) TLR3 deficiency in 2007, and, more recently, AD TNF receptor-associated factor 3 (TRAF3) and AR TLR3 deficiencies (10–13). Fibroblasts from patients with UNC-93B, TLR3, and TRAF3 deficiencies do not respond to stimulation with TLR3 agonists or infection with HSV-1 or vesicular stomatitis virus (VSV). HSE, together with other infectious diseases, was also reported in 2 children with mutations in STAT-1 and NEMO (10–15). These genetic deficiencies thus highlighted the importance of the TLR3-dependent production of IFN-α/β and IFN-λ after infection of the CNS with HSV-1 (6, 16, 17). In fibroblasts from patients with

Authorship note: Rebeca Pérez de Diego, Lazaro Lorenzo, Rabih Halwani, and Abdullah Alangari contributed equally to this work. Shen-Ying Zhang, Laurent Abel, and Saleh Al-Muhsen contributed equally to this work.

Conflict of interest: The authors have declared that no conflict of interest exists.

Citation for this article: *J Clin Invest.* 2011;121(12):4889–4902. doi:10.1172/JCI59259.

UNC-93B, TLR3, and TRAF3 deficiency (10–12) and in iPS-derived CNS cells (M. Lafaille, unpublished observations), impaired IFN production has been shown to result in enhanced viral replication and higher levels of cell death.

However, most cases of childhood HSE remain unexplained. We hypothesize that HSE is a genetically heterogeneous disease, involving a collection of single-gene inborn errors of immunity to HSV-1 in the CNS during the course of primary infection (18). Specifically, we hypothesize that mutations in genes controlling the TLR3 pathway may predispose children to HSE. Human TLR3-mediated immune responses are initiated by dsRNA intermediates in vivo or via their synthetic analog polyinosinic-polycytidylic acid [poly(I:C)] in vitro, leading to the induction of IFN-β via the NF-κB, IRF3, and AP-1 pathways (19). A principal candidate gene for HSE encodes the Toll/IL-1R (TIR) domain-containing adaptor inducing IFN-β (TRIF) protein, also known as TIR domain-containing adaptor molecule 1 (TICAM-1), due to its role as the sole adaptor of TLR3 (20–23). However, this molecule also serves as an adaptor for the MyD88-independent pathway downstream from TLR4 (24–26), raising the possibility that TRIF mutations may confer a distinct phenotype. A recent report has also shown TRIF to be involved in the detection of cytosolic dsRNA via the DExD/H-box helicase complex DDX1-DDX21-DHX36 (27). After TLR3 activation, TRIF is thought to act as a molecular platform for subsequent signaling events, recruiting TRAF3, TANK-binding kinase 1 (TBK1), NF-κB–activating kinase-associated protein 1, receptor-interacting protein 1 (RIP1), and IFN regulatory factor 3 (IRF3), in particular (28, 29). Mice lacking TRIF do not respond to poly(I:C), display impaired LPS-induced inflammatory cytokine production, and show increased susceptibility to mouse CMV and vaccinia virus infections (25, 26). Given the key role of TRIF in the TLR3 pathway demonstrated in mice, our previous demonstration of the role of the TLR3-IFN pathway in preventing the spread of HSV-1 to the CNS, and despite the potential involvement of human TRIF in TLR4 and helicase responses, we focused our candidate gene approach on TRIF by sequencing the *TRIF* gene in a cohort of children with HSE.

Results

Homozygous TRIF nonsense mutation in patient 1. A patient (P1) born to consanguineous Saudi parents presented HSE at the age of 2 years (Figure 1A). This patient is now 3.5 years old and has had no other unusually severe infectious disease. No mutations were found in the coding regions of *UNC93B1* and *TRAF3*, consistent with the normal PBMC responses to TLR3, TLR7, TLR8, and TLR9 agonists (leukocyte responses to TLR3 agonists have been shown to be TLR3 independent) observed in this patient (11, 13) (Supplemental Figure 1, A and B; supplemental material available online with this article; doi:10.1172/JCI59259DS1). No mutations were found in the coding regions of *TLR3*. However, both genomic DNA (gDNA) and cDNA from the leukocytes and fibroblasts of P1 displayed a homozygous nonsense mutation in *TRIF* at nucleotide position 421 (c.421C>T), resulting in a premature termination codon replacing an arginine residue at amino acid position 141 (R141X) (Figure 1, B and C). P1 is the proband and the only member of this family homozygous for this mutation. There are no other reports of premature termination mutations in *TRIF*, and this mutation was found neither in the NCBI or Ensembl databases nor in the 1,234 unrelated healthy controls sequenced, including 1,050 individuals from the Centre d'Etude du Polymorphisme Humain–Human Genome Diversity (CEPH-HGD) panel and 182 Saudi Arabian controls (a total of 2,464 chromosomes). The premature termination codon occurs at position 141, resulting in no detectable protein in SV40 fibroblasts and EBV-transformed B cells (EBV-B cells) from the patient, as shown by Western blotting (Figure 1D and Supplemental Figure 2A). *TRIF* mRNA levels in fibroblasts and EBV-B cells from P1 were similar to those in controls, as shown by quantitative real-time PCR (Q-PCR) and full-length TRIF RT-PCR, suggesting that there is little or no nonsense-mediated mRNA decay (Figure 1E and Supplemental Figure 2B). These data suggest that TRIF R141X is a null allele, causing complete TRIF deficiency in P1.

Heterozygous TRIF missense mutation in P2. A girl (P2) of mixed European descent (French, Portuguese, and Swiss) presented HSE at the age of 21 months (Figure 2A). The patient is now 18 years old and has had no other unusually severe infectious disease. Mutations in all known HSE-causing genes were excluded, not only for the coding regions of *UNC93B1* and *TRAF3*, consistent with the normal responses to TLR3, TLR7, TLR8, and TLR9 agonists observed (Supplemental Figure 1, C and D), but also for the coding regions of *TLR3*. However, both gDNA and cDNA from the leukocytes and fibroblasts of P2 displayed a heterozygous nucleotide substitution in *TRIF* at position 557 (c.557C>T), resulting in the substitution of a leucine for a serine residue at amino acid position 186 (S186L) (Figure 2, B and C). P2 is the proband and the only member of this family to have developed HSE. However, the mother and maternal grandfather of P2 also carry the S186L mutation and have HSV-1–specific serum antibodies. This mutation was not found in the NCBI and Ensembl databases or in the 1,050 unrelated healthy controls from the CEPH-HGD panel sequenced, including 289 Europeans (a total of 2,100 chromosomes). Serine 186 is conserved in 8 out of the 11 animal species with TRIF proteins sharing over 50% homology to the human protein (Figure 1D). Leucine has never been found in position 186 in any species, although 2 nonhuman primates and the horse carry an alanine residue at this position, whereas the mouse has a proline residue. The S186L mutation affects the N-terminal region of the protein (Figure 1C). Previous studies have shown that the N-terminal region of TRIF plays an important role, as an N-terminal deletion mutant (including S186) displayed a specific loss of IRF3 activation and IFN-β promoter induction (21, 25). *TRIF* mRNA and protein levels in the fibroblasts and EBV-B cells of P2 were found to be similar to those in controls, suggesting that the transcription and expression of the gene were not affected by this or any other undetected mutation (Figure 1, E and F, and Supplemental Figure 2, A and B). These data suggest that TRIF S186L is a rare allele and that the missense mutation may cause an AD form of TRIF deficiency, conferring a predisposition to HSE with incomplete clinical penetrance (similar to both UNC-93B and TLR3 deficiencies) (10, 11).

Impaired cellular responses to TLR3 agonists. Dermal fibroblasts from P1 and P2 were used to investigate the AR R141X and AD S186L *TRIF* mutations. After 24 hours of stimulation with poly(I:C), the fibroblasts of P1 and P2 displayed impaired production of IFN-β, IFN-λ1/3 (IL-29/IL-28B), and IL-6 similar to that observed in cells from UNC-93B–deficient patients and contrasting with the situation in cells from a healthy control ($P < 0.05$ for all comparisons) (Figure 3A). Cells from another TRIF heterozygote, the mother of P2, also showed impaired production of IFN-β, IFN-λ1/3, and IL-6 compared with that of a control ($P < 0.05$ for all comparisons) after

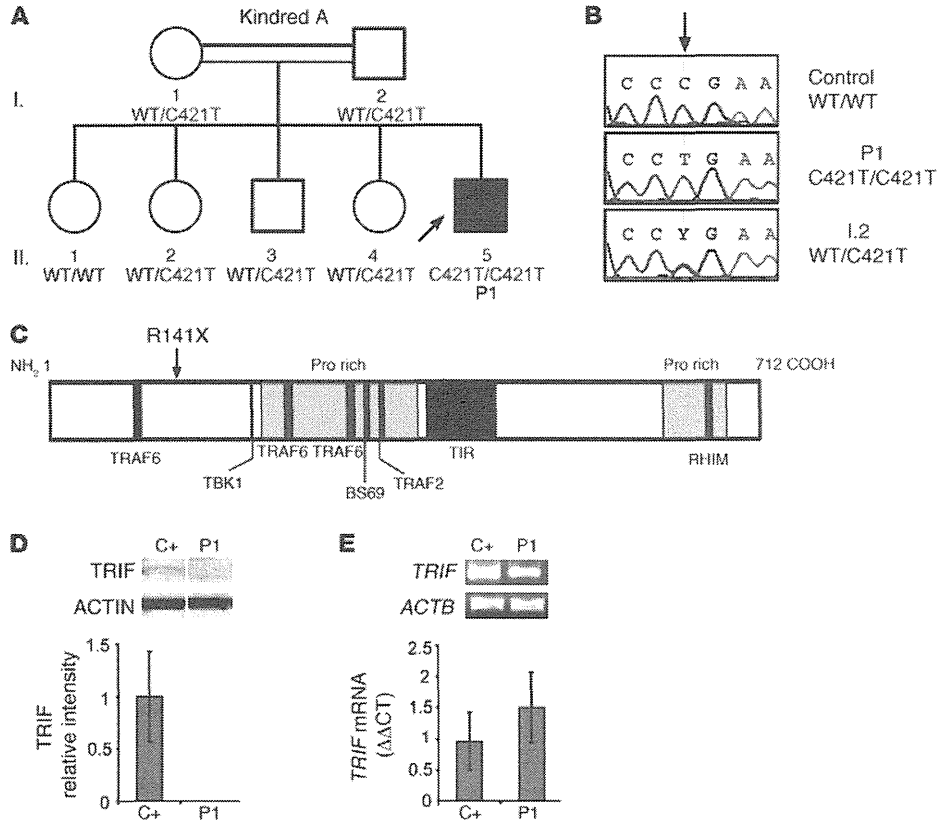

Figure 1

AR TRIF deficiency in P1. (**A**) Family pedigree of kindred A with allele segregation of the mutation. The HSE patient is shaded in black. Roman numerals (left margin) indicate generations. An arrow indicates the proband. (**B**) Automated sequencing profiles for the TRIF C421>T mutation in gDNA isolated from leukocytes from a healthy unrelated control; the patient, P1; and the father, I.2. The arrow indicates the position of the mutation. (**C**) A schematic representation of the TRIF protein (1–712 amino acids) indicating the amino acid position, R141X, affected by the C421>T mutation. Proline-rich domains (pro rich) are shaded in gray; functional domains are shaded in black (TRAF6 binding, TIR, RIP homotypic interacting motif [RHIM]). (**D**) TRIF protein expression by immunoblot analysis of SV40 fibroblast cell lysates from a healthy control (C+) and P1. Samples were migrated on the same blot. TRIF expression levels were quantified by densitometry results normalized with respect to ACTIN levels and expressed as relative intensity of TRIF. This is a representative blot from 3 independent experiments (mean ± SEM). (**E**) RT-PCR of full-length *TRIF* cDNA is shown with *ACTB* cDNA as an internal control. *TRIF* cDNA levels were assessed by real-time PCR in control fibroblasts (C+) and P1. Data are represented as relative fold change (ΔΔCt units), where *GUS* was used for normalization. An average of 3 independent experiments is represented (mean ± SEM).

24 hours of stimulation with various doses of poly(I:C) (Supplemental Figure 3). Consistent with the lack of IFN-β induction in P1, no IRF3 dimers were found in P1 or in cells from a patient with complete UNC-93B deficiency (negative control). In P2, IRF3 dimerization in response to poly(I:C) was impaired but not abolished. By contrast, cells from a patient with MyD88 deficiency and cells from a healthy individual (positive control) were able to form dimers as early as 1 hour after stimulation (Figure 3B). Nuclear translocation of the p65 subunit of NF-κB after poly(I:C) stimulation was also abolished in P1 cells ($P < 0.05$) and reduced in P2 cells ($P < 0.05$) compared with that in a control (Figure 3C). However, NF-κB activation in P1 and P2 cells was normal after stimulation with IL-1β and TNF-α. As expected, there was no p65 translocation upon IL-1β stimulation in MyD88-deficient cells or in NEMO-deficient cells. We then tested the responses of P1 and P2 to a specific noncommercial TLR3 agonist, polyadenylic-polyuridylic acid [poly(A:U)], poly(I:C) delivered intracellularly with lipofectamine, and the RIG-I–specific ligand, 7sk-as (30). There was no response to the TLR3 agonist poly(A:U) in P1 and P2 cells, whereas IFN-β, IFN-λ1/3, and IL-6 were induced in cells from P1 and P2 after transfection with poly(I:C) or 7sk-as (Figure 3D). Interestingly, both patients induced lower levels of IFN-β and IL-6 in response to transfected poly(I:C) compared with those of a control ($P < 0.05$ for all comparisons). Intracellular poly(I:C) is known to activate cytosolic dsRNA receptors, such as RIG-I and MDA5, which use the adaptor VISA to induce IRF3 and IFN-β (31, 32). Recently, however, TRIF was also shown to participate in cytosolic dsRNA receptors pathways (27). These findings demonstrate that the recognition of extracellular dsRNA was impaired in P1 and P2 cells, consistent with the established role of TRIF in the TLR3 pathway. The response to intracellular dsRNA in the cytosol was modestly affected in both patients, in line with recent reports of TRIF's involvement in cytosolic pathways. In addition, we carried out genome-wide transcriptional analysis of the TLR3 pathway

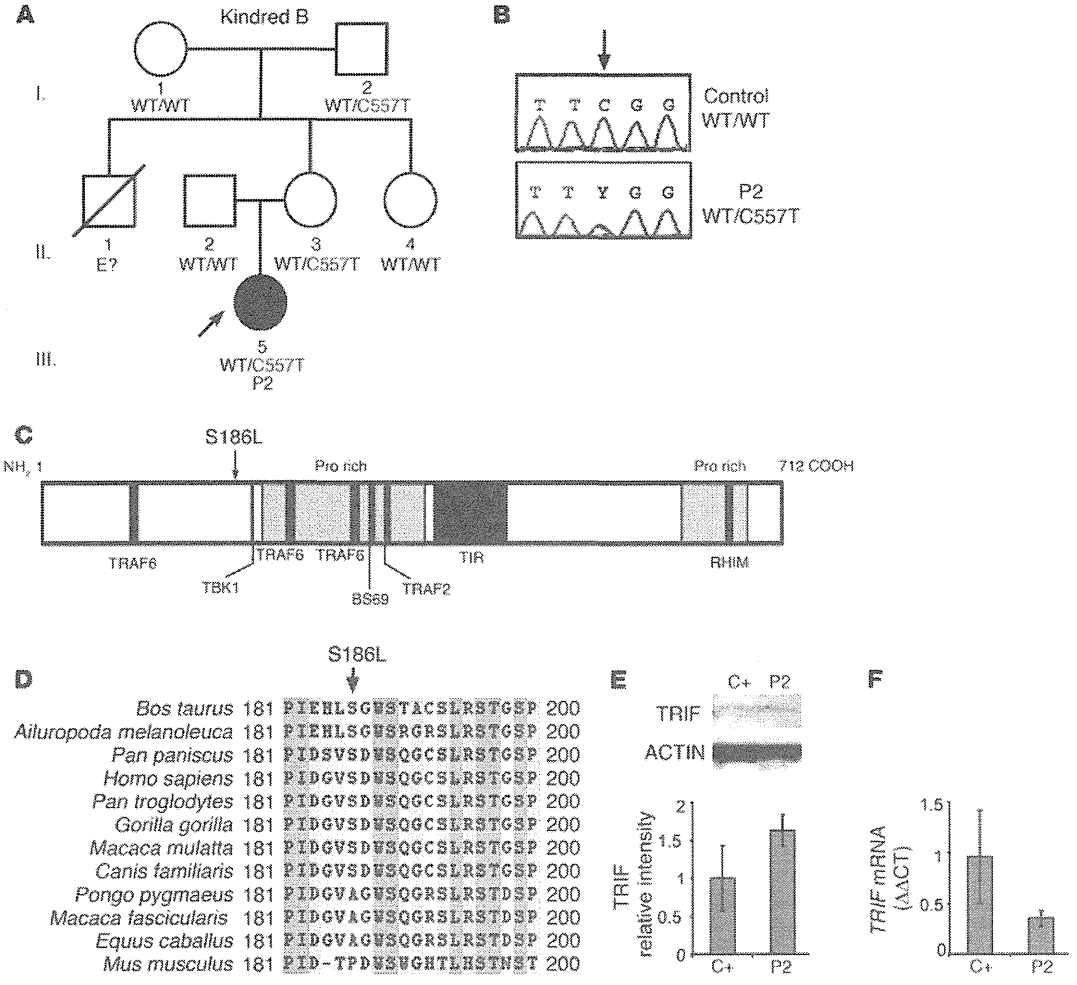

Figure 2

AD TRIF deficiency in P2. (**A**) Family pedigree of kindred B with allele segregation of the mutation. The HSE patient is shaded in black. Roman numerals (left margin) indicate generations. An arrow indicates the proband, and "E?" indicates an undetermined genotype. (**B**) Automated sequencing profiles for the TRIF C557>T mutation in gDNA isolated from leukocytes from a healthy unrelated control and in the patient, P2. The arrow indicates the position of the mutation. (**C**) A representation of the TRIF protein (1–712 amino acids) indicating the amino acid position, S186L, affected by the C557>T mutation. Proline-rich domains are shaded in gray; functional domains are shaded in black (TRAF6 binding, TIR, and RHIM). (**D**) Multiple alignment of TRIF amino acid sequence surrounding the mutation S186L. (**E**) TRIF protein expression by immunoblot analysis of SV40 fibroblast cell lysates from a healthy control (C+) and P2. TRIF expression levels were quantified by densitometry results normalized with respect to ACTIN levels and expressed as relative intensity of TRIF. This is a representative blot from 3 independent experiments (mean ± SEM). (**F**) *TRIF* cDNA levels were assessed by real-time PCR in control fibroblasts and P2. Data are represented as relative fold change (ΔΔCt units), where *GUS* was used for normalization. An average of 3 independent experiments is represented (mean ± SEM).

in fibroblasts of a control, P1, an AR TLR3-deficient patient, and an AR MyD88-deficient patient after 4 hours of poly(I:C) or IL-1β stimulation. In control fibroblasts, there were 506 transcripts found to be differentially regulated upon poly(I:C) (Supplemental Figure 4A). Unlike control cells or MyD88-deficient cells, P1 cells as well as the TLR3-deficient cells failed to respond to poly(I:C) (Supplemental Figure 4A), whereas their responses were normal upon IL-1β stimulation, unlike MyD88-deficient cells (Supplemental Figure 4B). Investigation of the functional pathways induced by poly(I:C) lead to the identification of genes that were induced in control cells but not in P1. These genes included IFN-regulated genes (*IFIH1*, *IFIT1*, *IFIT2*, and *IFIT3*), proinflammatory cytokines (*IFNB1*, *IL12A*, *IL15*, *IL29*, *TNFSF13B*, *TNFAIP6*, and *TNFSF10*), chemokines (*CXCL11*, *CCL3*, *CCL3L1*, *CCL3L3*, *CCL8*, *CXCL9*, *CCL5*, and *CXCR7*), and cell death/apoptosis genes (*RIPK2*, *BCL10*, *CASP7*, *BIRC2*, and *BIRC3*) (Supplemental Figure 4C). These experiments suggest that the R141X mutation results in a null allele causing AR complete TRIF deficiency, whereas the S186L *TRIF* allele is dysfunctional and causes AD dominant partial TRIF deficiency.

Cellular response to LPS. TRIF is known to interact with TLR4 in mice and humans (22) and has been shown to control IFN induc-

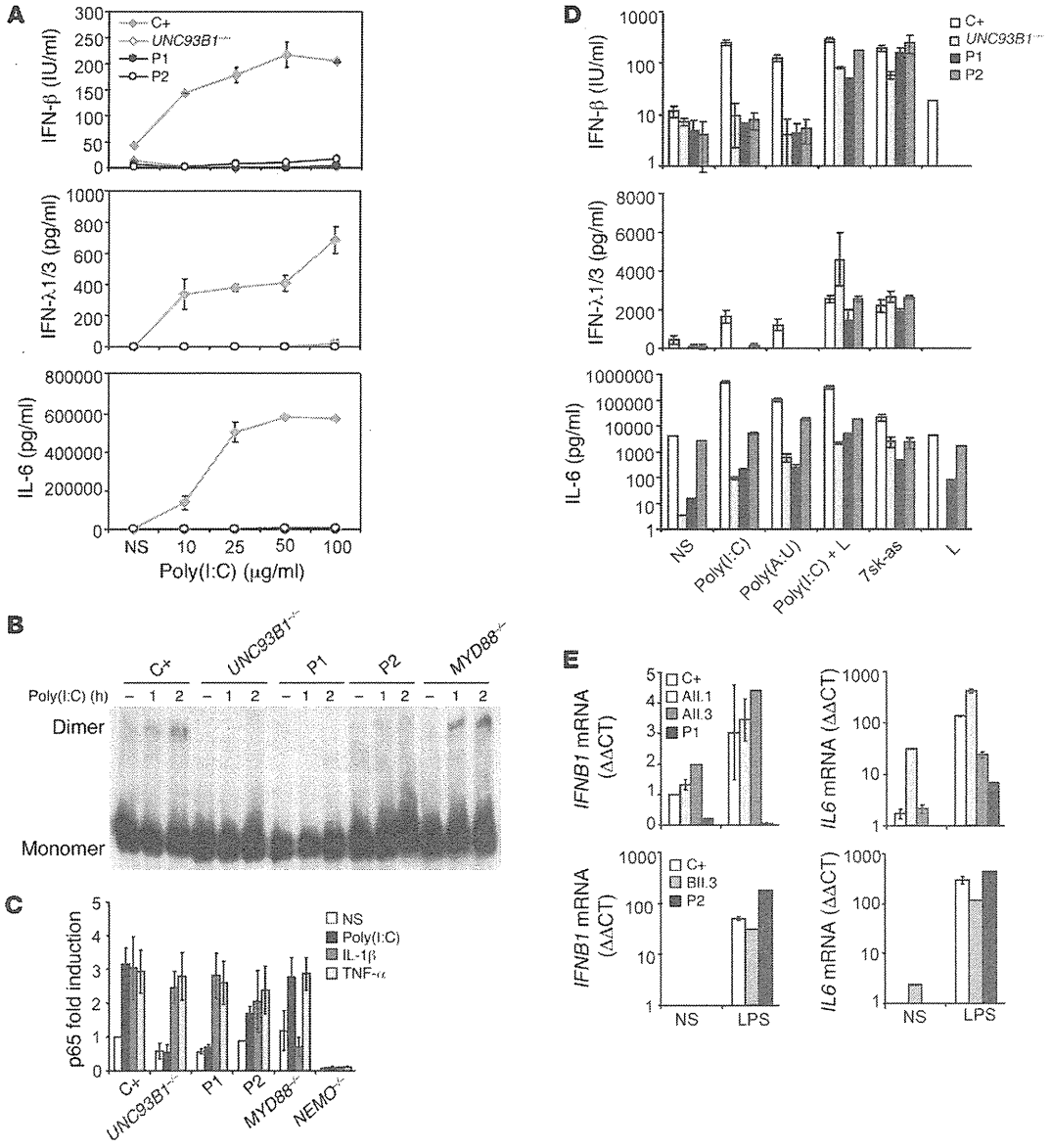

Figure 3

Response to TLR3 and TLR4 ligands. (**A**) SV40 fibroblasts were stimulated with increasing doses of poly(I:C) for 24 hours, and production of cytokines was assessed. C+ is a healthy control; *UNC93B1*$^{-/-}$ served as a negative control. Values (mean ± SEM) were calculated from 3 independent experiments. (**B**) Native gel Western blot showing IRF3 dimers from total fibroblast cell lysates after stimulation with poly(I:C) for 1 or 2 hours. C+ and *MYD88*$^{-/-}$ cells were used as positive controls to poly(I:C) stimulation, and *UNC93B1*$^{-/-}$ was used as a negative control. (**C**) Nuclear protein extracts from SV40 fibroblasts stimulated for 30 minutes with IL-1β or TNF-α and 120 minutes with poly(I:C) were tested for the presence of the p65 subunit of NF-κB by ELISA. *NEMO*$^{-/-}$ cells were used as a negative control for all stimuli; *MyD88*$^{-/-}$ was used as a negative control for IL-1β; and *UNC93B1*$^{-/-}$ was used for poly(I:C) stimulation. Values (mean ± SEM) were calculated from 3 independent experiments. NS, nonstimulated. (**D**) SV40 fibroblasts were stimulated with a TLR3-specific ligand, poly(A:U), transfected poly(I:C), RIG-I–specific ligand (7sk-as), or lipofectamine alone (L) for 24 hours and tested for cytokine production. Values (mean ± SEM) were calculated from 3 independent experiments. (**E**) PBMCs from healthy controls, various family members from kindred A (AII.1 and AII.3) and B (BII.3), and P1 and P2 were stimulated with LPS for 2 hours. Induction of *IFNB1* and *IL6* mRNA was assessed by real-time PCR. Values are expressed as relative fold change using the ΔΔCt method, where *GUS* was used for normalization; values (mean ± SEM) from 3 independent experiments were calculated.

tion by LPS in the mouse model (24–26). We therefore assessed *IFNB1* mRNA induction in response to LPS stimulation in PBMCs from the patients. Compared with those from with a healthy control or his WT or heterozygous siblings, PBMCs from P1 did not induce the production of *IFNB1* mRNA ($P < 0.05$, $P < 0.05$, and $P < 0.05$, respectively), whereas IL-6 was induced, albeit to a lower extent than in the control ($P < 0.05$), probably via the intact TLR4-MYD88–dependent pathway in P1 (Figure 3E). PBMCs from P2